COO-3072-13

Princeton University
Elementary Particles Laboratory
Department of Physics

A MEASUREMENT OF THE CHARGE ASYMMETRY IN $K_L^o \rightarrow \pi^{\pm} e^{\mp} \nu$ DECAYS

ROBERT CARROLL WEBB

TECHNICAL REPORT NO. 3

June 1972

Contract AT(11-1)-3072

A MEASUREMENT OF THE CHARGE ASYMMETRY IN $K_L^o \to \pi^{\pm} e^{\mp} \nu$ DECAYS

Robert Carroll Webb

A DISSERTATION

PRESENTED TO THE

FACULTY OF PRINCETON UNIVERSITY

IN CANDIDACY FOR THE DEGREE

OF DOCTOR OF PHILOSOPHY

RECOMMENDED FOR ACCEPTANCE BY THE

DEPARTMENT OF

PHYSICS

JUNE, 1972

TABLE OF CONTENTS

ABSTRACT

Using a magnetic spectrometer with multiwire proportional chambers for track definition, approximately $96*10^6$ $K_L^o \to \pi^{\mp} e^{\pm} \nu$ events were observed. From these K_{e3} decays the asymmetry in the decay rates for the two charge configurations was measured. This asymmetry was observed with three different mass configurations in the detector and an extrapolation to zero mass was performed. The result of this measurement is

$$\delta = \frac{\Gamma(K_L^o \to e^+\pi^-\nu) - \Gamma(K_L^o \to e^-\pi^+\nu)}{\Gamma(K_L^o \to e^+\pi^-\nu) + \Gamma(K_L^o \to e^-\pi^+\nu)}$$

$$= (2.66 \pm .34)*10^{-3} \quad .$$

In terms of the parameters ε usually used to parameterize CP violation in the neutral K system this result leads to a measure of

$$\mathrm{Re}\varepsilon = (1.33 \pm .17)*10^{-3}$$

in the limit that $\Delta S = -\Delta Q$ amplitudes are zero. The most recent results for $|\eta_{+-}|$, $|\eta_{oo}|$, and their phases, ϕ_{+-} and ϕ_{oo}, lead to a predicted $\mathrm{Re}\varepsilon$ of,

$$\mathrm{Re}\varepsilon = (1.45 \pm .09)*10^{-3}.$$

CHAPTER I

INTRODUCTION AND THEORY

The first observation of the CP violating decay of $K_L^o \to \pi^+\pi^-$ by Christenson, Cronin, Fitch, and Turlay[1] has led to a spate of theories[2] and experiments[3] which have been directed toward understanding this phenomenon. To date, the only manifestations of CP violation to be observed have been in the neutral kaon system. In order to explore further the details of CP violation as observed in the decay of the neutral K meson a precision experiment was performed, the results of which could be used as a consistency check on the interrelationship of several independent measurements which have been made on the $K^o - \overline{K}^o$ system. The experiment was to measure the charge asymmetry in the semi-leptonic decay, $K_L^o \to \pi^\pm e^\mp \nu$. By measuring this charge asymmetry one acquires information which when coupled with the other experimental measurements on the neutral K system, overdetermines the magnitudes and phases of ϵ and ϵ', quantities first introduced by Wu and Yang[4] to parameterize CP violation. The experiment thus provides a test of the validity and consistency of the assumptions that were made in the parameterization, e.g., CPT invariance. In addition, as has been emphasized by Bell and Zia[5], and independently by Brodine[6], a sensitive measure of the variation of the charge asymmetry across the Dalitz plot provides a measure of other CP violating parameters. Thus, another motivation for this experiment was to make a preliminary assessment of the difficulties of such a refined measurement.

The results of previous experiments[7-11] are listed in Table I. The two most significant efforts, statistically speaking, were performed under similar experimental conditions and were not in agreement. These two measurements were characterized by substantial corrections for the mass of the detector (in the

latest result the correction almost doubled the measured asymmetry). This leads one to pay particular attention to the possible systematic errors attendant with this experimental problem. Before going into the details of the experiment, a brief discussion of the theory of the K^o- $\bar{K}^o$ system is in order.

A. The Quantum Mechanical 2 State System

Since the kaon is the lowest mass particle with strangeness[12], it must decay via strangeness-violating interactions into pions, electrons, muons, and gamma rays. These strangeness-violating "weak" decays make it possible for a K^o to make a virtual transition into $\bar{K}^o$ and <u>vice versa</u>, e.g.,

$$K^o \leftrightarrows \begin{matrix} 2\pi \\ 3\pi \\ \pi e \nu \end{matrix} \leftrightarrows \bar{K}^o$$

and as a result, two new basis states emerge[13]. Using the Wigner-Weiskopf[14] reduction, the time dependence of the K^o-$\bar{K}^o$ system is described in terms of an "effective Hamiltonian", viz.,

$$-i \frac{d}{dt} \psi = H_w \psi$$

with

$$H_w = \begin{pmatrix} r & p^2 \\ q^2 & s \end{pmatrix} \qquad \text{(I.1)}$$

where

$$\psi(t) = a(t)|K^o\rangle + b(t)|\bar{K}^o\rangle = \begin{pmatrix} a(t) \\ b(t) \end{pmatrix}$$

and where r = s with CPT invariance and no material present. The eigenvalues of this system are

$$\lambda_{1,2} = r \pm pq = M_{1,2} - i \frac{\Gamma_{1,2}}{2} \qquad \text{(I.2)}$$

and the eigenstates of the system are then simply

$$|K_1^o\rangle = p|K^o\rangle + q|\bar{K}^o\rangle$$
$$|K_2^o\rangle = p|K^o\rangle - q|\bar{K}^o\rangle. \tag{I.3}$$

This "effective Hamiltonian" H_w is decomposed into a mass and decay part

$$H_w = M - i\Gamma \tag{I.4}$$

where M takes into account the mixing of K^o and $\bar{K}^o$ via second order virtual weak transitions through its off-diagonal elements and which leads to the observed mass splitting for the two neutral kaon states of

$$\delta M = \frac{M_1 - M_2}{\hbar} = (-.539 \pm .0035)\ 10^{10}\ \text{sec}^{-1}. \tag{I.5}$$

The decay matrix, Γ, takes into account the transitions to observable physical states. The diagonal elements of the operator Γ reduce to a sum of the partial decay half rates.

If CP is conserved in the K^o-$\bar{K}^o$ system under these conditions, the operator CP should commute with the "effective Hamiltonian" i.e.

$$[H_w, CP] = 0 \tag{I.6}$$

and one expects CP to act on the K^o states as follows

$$CP \begin{pmatrix} K^o \\ \bar{K}^o \end{pmatrix} = \begin{pmatrix} \bar{K}^o \\ K^o \end{pmatrix}.$$

Then for this representation CP takes the form

$$CP = \begin{pmatrix} 0 & 1 \\ 1 & 0 \end{pmatrix}. \tag{I.7}$$

Requiring $[H_w, CP] = 0$ implies from equation (I.1) that $p^2 = q^2$ and this transforms (I.3) into the well-known set of CP eigenstates

$$|K_1^o\rangle = \frac{1}{\sqrt{2}}(|K^o\rangle + |\bar{K}^o\rangle) \qquad CP + 1$$
$$|K_2^o\rangle = \frac{1}{\sqrt{2}}(|K^o\rangle - |\bar{K}^o\rangle) \qquad CP - 1 \quad . \tag{I.8}$$

However, when $[H_w, CP] \neq 0$, the physically observed states (i.e., those with definite lifetimes) of the K^o-$\bar{K}^o$ system are no longer the $|K_1^o\rangle$ and $|K_2^o\rangle$ shown above, by virtue of the Christenson et al. experiment, but are some slightly perturbed set of basis states that are noted as $|K_S^o\rangle$ and $|K_L^o\rangle$ with

$$|K_S^o(t)\rangle = p|K^o(t)\rangle + q|\bar{K}^o(t)\rangle = |K_S^o(o)\rangle e^{-i(M_S - i\frac{\Gamma s}{2})t}$$
$$|K_L^o(t)\rangle = p|K^o(t)\rangle - q|\bar{K}^o(t)\rangle = |K_L^o(o)\rangle e^{-i(M_1 - i\frac{\Gamma 1}{2})t} \tag{I.9}$$

and $p \neq q$. Having established this distinction one can now write down explicitly the relevant expressions for the observed CP violating quantities appearing in the neutral K^o system.

B. CP Violation

The first manifestation of CP violation was the measurement of non-zero amplitude for $K_L^o \to \pi^+\pi^-$ [1]

$$\eta_{+-} = \frac{\text{amp.}(K_L^o \to \pi^+\pi^-)}{\text{amp.}(K_S^o \to \pi^+\pi^-)} \quad . \tag{I.10}$$

One can write the amplitudes of K^o and $\overline{K}^o$ in $(2\pi, J=0)$ states with isotopic spin I as follows

$$\sqrt{\rho_{2\pi}}\ a_I(K^o) = e^{i\delta_I} A_I$$
$$\sqrt{\rho_{2\pi}}\ a_I(\overline{K}^o) = e^{i\delta_I} A_I^* \qquad (I.11)$$

with $\rho_{2\pi}$ representing the density of final states of the 2π system. Then

$$\text{amp.}(K^o_{L,S} \to \pi^+\pi^-) = e^{i\delta_0}\, p(\sqrt{2}/3\, A_0 + 1/\sqrt{3}\ A_2 e^{i(\delta_2-\delta_0)}) \mp q(\sqrt{2}/3\, A_0^* + 1/\sqrt{3}\ A_2^* e^{i(\delta_2-\delta_0)})$$

which yields

$$\eta_{+-} = \frac{p(\sqrt{2}/3\, A_0 + 1/\sqrt{3}\, A_2 e^{i(\delta_2-\delta_0)}) - q(\sqrt{2}/3\, A_0^* + 1/\sqrt{3}\, A_2^* e^{i(\delta_2-\delta_0)})}{p(\sqrt{2}/3\, A_0 + 1/\sqrt{3}\, A_2 e^{i(\delta_2-\delta_0)}) + q(\sqrt{2}/3\, A_0^* + 1/\sqrt{3}\, A_2^* e^{i(\delta_2-\delta_0)})} \qquad (I.12)$$

Choosing A_0 to be real after Wu and Yang [4], gives the following to first order

$$\eta_{+-} = \frac{p-q}{p+q} + 1/\sqrt{2}\ \frac{(A_2-A_2^*)}{A_0}\ e^{i(\delta_2-\delta_0)} + \ldots. \qquad (I.13)$$

which may be written as

$$\eta_{+-} = \varepsilon + \varepsilon' \qquad (I.14)$$

where

$$\varepsilon \equiv \frac{p-q}{p+q} \qquad (I.15)$$

$$\varepsilon' \equiv i/\sqrt{2}\ \frac{\text{Im}(A_2)}{A_0}\ e^{i(\delta_2-\delta_0)} \qquad (I.16)$$

This form of parameterization has the advantage of isolating the contributions of CP violation into the I = 0 and I = 2 parts and relating the measured

quantities η_{+-} and η_{oo} rather directly to the elements of the mass decay matrix H_w. In the same way one can express the quantity η_{oo} as,

$$\eta_{oo} = \frac{\text{amp.}(K_L^o \to \pi^o\pi^o)}{\text{amp.}(K_S^o \to \pi^o\pi^o)} = \varepsilon - 2\varepsilon' \quad . \tag{I.17}$$

Focusing on the lepton charge asymmetry, one defines the four amplitudes for the decay, while allowing for possible violation of the selection rule $\Delta S = \Delta Q$, as:

$$\begin{aligned} &\langle \pi^- e^+ \nu | H_w | K^o \rangle = f \\ &\langle \pi^+ e^- \bar{\nu} | H_w | \bar{K}^o \rangle = f^* \\ &\langle \pi^- e^+ \nu | H_w | \bar{K}^o \rangle = g \\ &\langle \pi^+ e^- \bar{\nu} | H_w | K^o \rangle = g^* \quad . \end{aligned} \tag{I.18}$$

Representing the amount of violation of the $\Delta S = \Delta Q$ rule by the quantity $x = g/f$, the decay rates for a pure K_L^o beam into the states $e^+\pi^-\nu$ and $e^-\pi^+\bar{\nu}$ are

$$\begin{aligned} N^+(K_L^o \to \pi^- e^+ \nu) &= |pf - qg|^2 \\ &= \frac{|f|^2 \, |p+q|^2}{4} \{ |1-x|^2 + (1-|x|^2)\, 2\text{Re}\varepsilon - 4\text{Im}x \, \text{Im}\varepsilon \} \end{aligned} \tag{I.19}$$

and

$$\begin{aligned} N^-(K_L^o \to \pi^+ e^- \bar{\nu}) &= |pg^* - qf^*|^2 \\ &= \frac{|f|^2 \, |p+q|^2}{4} \{ |1-x|^2 - (1-|x|^2)\, 2\text{Re}\varepsilon - 4\text{Im}x \, \text{Im}\varepsilon \} \quad . \end{aligned} \tag{I.20}$$

Combining these, the charge asymmetry becomes

$$\delta = \frac{N^+ - N^-}{N^+ + N^-} = 2\text{Re}\varepsilon \, \frac{1-|x|^2}{|1-x|^2} \tag{I.21}$$

which in the limit of $x \ll 1$, which agrees well with present experimental results [15], becomes

$$\delta = 2\text{Re}\varepsilon \quad . \tag{I.22}$$

Given the symmetry of CPT in the K^o-$\overline{K}^o$ system, a measurement of the charge asymmetry then provides a direct measure of the non-orthogonality of the physical K^o states by virtue of equations (I.9) and (I.15). This can be illustrated through an expression of the states of the K_L^o and K_S^o using the parameter ε as follows:

$$|K_L^o\rangle = \frac{|K_2^o\rangle + \varepsilon|K_1^o\rangle}{(1 + |\varepsilon|^2)^{\frac{1}{2}}} \qquad (I.23)$$

$$|K_S^o\rangle = \frac{|K_1^o\rangle + \varepsilon|K_2^o\rangle}{(1 + |\varepsilon|^2)^{\frac{1}{2}}}$$

Then it follows trivially that to first order in ε

$$\langle K_L^o|K_S^o\rangle = 2Re\varepsilon \quad . \qquad (I.24)$$

C. Estimate of $\langle K_L^o|K_S^o\rangle$

Lee, Oehme, and Yang (1957)(16) invoked unitarity to make an estimate of the upper limit of this non-orthogonality of the two states. From the previous discussion of the "effective Hamiltonian" of the K^o system, the aspect of the decay of the states has been included via the presence of Γ. Since unitarity requires the conservation of probability for a state, by evaluating the following differential equation for the K^o- $\overline{K}^o$ states

$$-\frac{d}{d\tau}|\psi|^2 = \sum_f \langle\psi|H_w|f\rangle\langle f|H_w|\psi\rangle$$

where ψ is the two component wave function (I.25)

$$|\psi\rangle = a_s|K_S^o(\tau)\rangle + a_l|K_L^o(\tau)\rangle$$

one arrives at the following result

$$|\langle K_L^o|K_S^o\rangle| < \sum_f \frac{\sqrt{\Gamma_{Lf}}\ \sqrt{\Gamma_{Sf}}}{(\lambda_L^* - \lambda_S)} \qquad (I.26)$$

where $\lambda_L^* - \lambda_S \sim \delta M$ the $K_L^o - K_S^o$ mass difference.

At the present time all the experimental rates have not yet been measured, but by using present values from existing experiments, Equation (I.26) can be evaluated in a fashion similar to Bell and Steinberger [17] and later Gourdin and Charpak [18]. These calculations include only the 2π decay mode which dominates the process. However, when considering all possible connecting intermediate states of the neutral K system, one arrives at the following result,

$$|\langle K_L^o | K_S^o \rangle| < (7.43 \pm .20) * 10^{-3}.$$

The data for this calculation are presented in Table II.

CHAPTER II

APPARATUS

In setting out to perform this sensitive measurement on the K_{e3} system, great care was taken in minimizing possible sources of systematic error or bias in the result. The basically simple task of lepton identification and charge determination, which is all that need be measured in this experiment, is to be contrasted to the complex dependence of the measured asymmetry on the material present, the symmetry of the detector, and instrumental biases. In order to minimize the effect of these biases the spectrometer was designed to be as symmetrical as possible, to have as low a mass as possible, and to be highly stable against fluctuations in detection efficiency. The absorption of the π^+ and π^- mesons resulting from K_{e3} decay are, to a first approximation, similar in isotopically pure materials. For this reason the detector was additionally designed to be as isotopically pure as possible.

A. Beam

The beam layout for this experiment at the Brookhaven Alternating Gradient Synchrotron (AGS) is shown in Fig. 1. During this experiment there were, on the average, 10^{12} protons incident on the target in the G-10 straight section per AGS pulse every 2.3 seconds. A neutral secondary beam at -20^{o} with respect to the internal beam direction was defined by a set of three 4-feet long Pb collimators with brass inserts combined with a magnet to remove charged particles. The location of these collimators is given in Table III. The sweeping magnet, located between collimators 1 and 2, was operated with a minimum field integral

of 400 Kgauss-inches. During the running of the experiment the field value of this sweeping magnet was varied above this minimum value with no discernable effect on the experimental rates.

Each of the three collimators contained a tapered brass insert which pointed back to the target in the vertical direction and to a point 25 inches in back of the target in the horizontal. The arrangement of these collimators was chosen in order to minimize the sensitivity of the apparatus to target position during running. A limiting aperture of 60.7 μsteradians was imposed by the defining aperture of the collimator furthest downstream.

The beam's constituents were primarily long-lived neutral particles (e.g., neutrons, γ-rays, and K_L^o mesons). The γ-rays were attenuated by passage through a 10 radiation length Pb filter placed immediately upstream of collimator 1. The relatively low ratio of neutrons to K_L^o's in the beam of 10:1 was a consequence of the arrangement of the beam line to be well outside the neutron diffraction peak. The fact that these neutron fluxes were at a relativley low level reduced the background due to neutron interactions to a manageable level.

The observed K_L^o decays were consistent with a nearly uniform illumination of the beam cross sectional area throughout the length of the decay region. The K_L^o production spectrum at the target was

$$f(p) \propto p \exp(-p \sin\theta_{beam}/\langle p_\perp \rangle)$$

where $\langle p_\perp \rangle$ = 190 MeV/c for p > 800 MeV/c for this beam angle. This parameterization of the momentum spectrum was a result from a previous experiment carried out in this beam line (Ref. 19).

B. Spectrometer

A plan view of the spectrometer geometry is given in Fig. 2. A typical event was one in which a K_L^o decays in the helium filled region between counter E and chamber 2 into $\pi^{\pm}e^{\mp}\nu$, where the spectrometer was sensitive to the charged pair only. One of the charged particles was required to traverse the spectrometer on each side of the beam axis, resulting in a pair of signals in coincidence from each of the five proportional chambers and the back hodoscope bank. The identification of the electron was accomplished by a threshold Čerenkov counter located between chamber 3 and the magnet. Thus, under normal running conditions, the K_{e3} signature was established by the presence of a Čerenkov signal in coincidence with two signals from the back hodoscope banks and two tracks in the proportional chambers.

(1) The Magnet

At the heart of the apparatus was a (72D18-MKII) dipole magnet of the picture frame design, having a 72-inch wide by 18-inch high aperture with an effective field length of 30 inches. During the running of this experiment the central field value was set at 4.82 Kgauss, which corresponds to a value for the field integral of

$$\int B \cdot dl = 116.0 \text{ MeV/c.}$$

In order to cancel out any residual systematic left-right asymmetry of the apparatus, the polarity was changed after every 200 K triggers which was approximately every 2 hours during normal running. The total experiment involved $\sim$ 500 such field reversals.

(2) The Proportional Chambers

Since the measured asymmetry is so sensitive to the presence of material

the design for this experiment required a minimum mass detector. In order to achieve this, the primary particle detectors were multiwire proportional chambers. The very appealing features of these devices were:

(a) their good time resolution,

(b) their very low mass, $\lesssim$ 50 mg/cm^2 per chamber,

(c) their high efficiency for particle detection (both for pions and electrons).

The design of these chambers followed along the lines of the work done recently by Charpak et al.[20] in their revitalization of the proportional counting technique.

The locations and other pertinent data for the five chambers used in the experiment are shown in Table IV. These chambers were constructed by winding wires vertically onto a pair of fiberglass frames. After gluing the wires to the fiberglass, the two frames were placed together to form a three layer sandwich of parallel wire planes. The wire spacing was 1/8-inch and the interplane spacing was 1/4-inch[21]. Windows of .002-inch Aclar were placed on the outer faces of the chamber frame to form a gas seal for the chamber. Each chamber was flushed continuously with a mixture of $\sim$ 66.4% Argon, $\sim$ 33.4% CO_2, and $\sim$.25% Freon 13-B1 at a rate such that the chamber volume was displaced every 2 hours. After having operated these chambers $\sim$ 1000 hours in radiation intensities of up to > 10^6 part/sec., there has been no sign of degradation of chamber performance.

The electronic detection and readout system developed for use with these chambers had several unique features and is shown schematically in Fig. 3. The initial stage of the detection circuit was a Fairchild μA733 differential amplifier with a gain of 200. Wired to the inputs of these amplifiers were groups

of several wires (see Table IV and Fig. 4) which, when combined, made resolution elements varying from 3/4 inches to 1-1/8 inches in width. The increased capacitance, which resulted operating in this mode, necessitated the high gain amplifier. The amplifier-discriminator combination was adjusted such that a 250 μ-volt input signal would trigger the discriminator. This sensitivity, coupled with the particular gas mixture used, resulted in plateaus of from 100-300 volts at 3.5-4.5 kV chamber voltage (depending on wire used) for both pions and electrons in all of the chambers, and these plateaus were observed to be stable to within ± 20 volts throughout the running of the experiment.

There were several compelling reasons for choosing this particular amplifying scheme over the other possible candidates under consideration at the design stage of this experiment. Since the chambers were to be operated with these resolution elements, the high gain requirement made the overall system susceptible to noise pick-up problems. However, by using a differential amplifier, which has a low common mode gain, in this way, the sensitivity to these stray electrical signals was minimized. In addition, by using this differential amplifier instead of a conventional single input amplifier one could also reduce the amount of electronics necessary by a factor of 2 to amplify the proportional chamber pulses thus providing a substantial saving in hardware cost.

Once a proportional signal was detected by an amplifier and a standard shape signal had been formed by its accompanying discriminator, it was transmitted to a conventional 16-bit tagging module via a twisted pair cable. The transit time of these signals down the cable was selected to allow for sufficient time to make a decision as to whether a K_{e3} decay had been observed. The use of this long cable as a delay provided $\sim$ 150 nsec to establish the fact that a K_{e3} decay had been observed without introducing the long dead times involved

in doing this electronically. When the trigger condition was satisfied a "load" signal, which was 120 nsec wide, was transmitted to each of the 14 tagging modules for the chambers, and any chamber discriminator signal arriving at the tagging module during this load window was flagged as "on" and saved for readout some microseconds later by a SAC MIDAS system[22].

The proportional chambers were used not only for track position information but also they were used to establish a trigger with the proper K_{e3} signature. The resolution time of the proportional counters in establishing the K_{e3} trigger was $\sim$ 120 nsec. This is to be compared with $\sim$ 1 μ second if spark chambers had been used.

(3) The Čerenkov Counter

To identify the lepton in the K_{e3} decay, a gas filled threshold Čerenkov counter was used with CO_2 at NTP as the radiator. This counter was very compact in design and had a measured electron detection efficiency of $\sim$ 99%. The construction and design of the counter are discussed in detail in Ref. 19 and relevant parameters appear in Table V. However, in order to adapt the counter to this experiment, two basic changes were made to minimize the mass of the counter. The first was the replacement of the 1/4-inch thick Plexiglas front surface spherical mirrors with ones which were 1/32-inch in thickness. These new mirrors were made by forming Plexiglas at elevated temperatures to the correct radius of curvature, then having them coated with a .15 μ layer of aluminum[23]. These mirrors provided a reflectivity of $\sim$ 90% from 2200 Å - 5200 Å, which covers the region of the photocathode response for the RCA 4522 5-inch bi-alkali phototubes used to view the Čerenkov light. The second modification was the installation of thin entrance and exit windows of .0025-inch aluminized Mylar. After making these modifications, the total material in the Čerenkov counter was .285 g/cm^2.

In order to evaluate possible sources of contamination of the K_{e3} measurement by the Čerenkov counter's sensitivity to other K_L^o decay modes, it is useful to point out the Čerenkov counter's sensitivity to detection of other high momentum particles. Carbon dioxide has an index of refraction of 1.00045 at 3200 Å and 15° C. This value corresponds to the following thresholds for detection of e, π, μ, and p via their Čerenkov radiation in this gas:

	E_K
electron	16 MeV
pion	4500 MeV
muon	3400 MeV
proton	30 GeV .

If one folds in the pion and muon momentum spectra from the observed K_L^o decays in this beam, the result is a dilution of the measured asymmetry via contamination from the $K_{\mu 3}$ and the $K_{\pi 3}$ modes of less than 1 part in 10^6.

The location of the Čerenkov counter in the spectrometer is shown in Fig.2. One of the many advantages of this geometry was the early tagging of the electron in its passage through the spectrometer. It can also be noted that by locating the counter upstream of the spectrometer magnet one achieves a higher K_{e3} event acceptance for a smaller counter volume. One of the more important features of this counter was the location of the phototubes in the symmetry plane of the spectrometer magnetic field, while at the same time being moved away from the central field region of the magnet. Typical field values in the region of these phototubes were $\lesssim$ 20 gauss before shielding. Having taken advantage of this design feature, magnetic shielding for these phototubes was simplified substantially. It was necessary to shield the tubes from the small fields normal to the axis of

the phototube, a relatively easy task. Due to the field geometry there can be no field component along the axis of the phototubes. Shielding phototubes against axial fields is difficult and avoiding these problems contributes further to eliminating a possible variation in electron detection efficiency as a function of magnet polarity. From pulse height measurements on this counter using a nanosecond light pulser, the effectiveness of the shielding was verified. As a further check on sources of systematic effects, pulse height spectra for each of the phototubes in the counter were taken periodically throughout the running period, and from these measurements it has been verified that there is further no evidence of any polarity dependence of the detection efficiency for electrons to better than 1 part in 10^5.

(4) Scintillation Counters

Due to the mass of solid scintillation materials this type of particle detector was avoided in the bulk of the apparatus. However, as mentioned earlier, the relatively poor time resolution of the proportional counters necessitated the sparing use of nanosecond resolution particle detectors. A single scintillation counter hodoscope, described in Table VI and shown in Fig. 3, served to terminate the detector system. It was composed of two banks of (4) Pilot-B scintillators[24] viewed from top and bottom by RCA 7746 phototubes. The signals from both phototubes were added actively to generate a signal for each hodoscope element. Fluctuations in timing due to light transit and collection times were minimized by this design.

The threshold for particle detection in these counters was decreased to 1/4 minimum ionizing level to reduce the effective detection thickness to 1/32 of an inch of scintillator for the pions and less for the electrons. These phototubes were located in regions of magnetic field of much less than 10 gauss.

However, to prevent any systematic effects of these small fields on their detection efficiency, the tubes were doubly shielded against magnetic fields with an inner shield of Mu metal and a 1/4-inch thick outer iron shield.

There were also 7 scintillation counters operated in anticoincidence in the spectrometer (Table VI). Six of these were out of the beam and used to tag particles which might have passed through regions of high mass near the magnet pole tips and yoke. There were two horizontal anticounters in front of the magnet labeled F_1 and F_8, and four counters used for vertical aperture definition behind the magnet labeled M_1- M_4. Events for which these counters were triggered were included in the raw data sample with the states of these counters recorded along with other data written on magnetic tape.

The seventh anticounter was a 15"x24"x1/16" scintillator viewed on opposite edges by two RCA 8575 phototubes. It was located 18 inches downstream of the third collimator and was used to define the upstream limit of the decay volume. During the bulk of the data taking, events which had this anti trigger in coincidence with an event were not recorded. However, the status of this counter was also part of the tagging information recorded for each event thus allowing correction to the data sample for effects due to inefficiencies and/or accidentals problems observed in this event triggering system. For $\sim$ 8% of the data this counter was removed from the logic requirement for triggering and its status was simply recorded for each event. This data allowed the effect of upstream contamination in the data sample due to possible inefficient counter performance to be evaluated.

C. Data Taking

(1) Criteria for Acceptable Event Trigger

In order to efficiently record data with the minimum amount of background

contamination, the following method was used to establish an event trigger. First, the signals from the back hodoscope counters and the Čerenkov counter were put into coincidence to provide a relatively loose 2 track signature with fast timing. This signal was then placed into coincidence with the fast logic signals from each of the proportional chambers, and only events where any 2 out of the 3 front chambers triggered on each side of the apparatus as well as both back chambers were accepted, viz.,

$$B_L \cdot B_R \cdot \check{C} \; (1L \cdot 2L \cdot 3L)_{2 \text{ out of } 3} (1R \cdot 2R \cdot 3R)_{2 \text{ out of } 3} (4L \cdot 4R) \; (5L \cdot 5R) \quad .$$

Once this requirement was fulfilled, the readout of the data tagging modules was initiated and the system was turned off for 6 μ sec while the information was collected and written as a 24 word, 16 bit/word record into a 4096 word data buffer. The contents of the buffer were placed on magnetic tape between each AGS beam cycle.

(2) On-Line Monitoring

There were several on-line monitoring facilities with this experiment which were extremely useful in tracking the stability of the apparatus. The major on-line monitor, aside from the physicist on shift, was a Hewlett-Packard HP2116B 16K word computer which was equipped with a small reconstruction program. As the data was accumulated during each AGS spill cycle, the computer read the data into a buffer area and, during the interval between beam spills, analyzed each event checking for consistency with K_{e3} signature and tabulating analysis efficiencies. In addition, the computer accumulated data on the frequency of each spectrometer element's "on-state" in the data words for each event. This feature was indispensable in the early stages of running for debugging noisy or inefficient electronics in the proportional chamber system.

The second monitoring device was the Čerenkov monitor. It is shown

schematically in Fig. 5. The function of this monitor was to scale the frequency of coincidence of full signature K_{e3} events with signals from each of the 4 Čerenkov tubes. This monitor thus provided a raw measure of the charge asymmetry and a very accurate monitor for apparatus asymmetries during running.

(3) Format of Primary Data

In order to preserve the maximum information for each event, a data format was adopted which recorded the states of all of the spectrometer's elements in the form of twenty-four sixteen-bit words. Words 1-4 were used for fixed data information on polarity, mass of spectrometer and tape number. Words 5 and 6 were used for scintillation counter tagging and a failsafe magnet polarity sensing readout which was connected directly to the coils of the magnet. Words 7-20 were used for tagging of each of the 14 words of chamber readout, and the last 4 words were used for an event counter and a neutron monitor scaler. For a block diagram of this data assembly, see Fig.6. During the running of the experiment, $96*10^6$ such events were recorded on $\sim$ 500 reels of 2400-feet, 7 track, 556 BPI magnetic tapes.

D. The Experimentally Determined Mass Correction

As was mentioned earlier one of the prime considerations in performing this asymmetry measurement was to minimize the net amount of material through which the K^o_L secondaries had to pass in order to be detected in the spectrometer. The reason for this consideration is straightforward and stems from the non-negligible effects of the positron annihilation cross section and the difference in the π^+ and π^- nucleus absorption and scattering cross sections. These effects result in a differential absorption in the spectrometer for the two pertinent decay channels. In addition the presence of mass in the decay volume can lead

to the production of particles whose β decay is completely charge asymmetric, e.g., Λ^o's.

In previous charge asymmetry experiments two approaches had been employed to make this correction to the data. The first method was to calculate the differential absorption by using known empirical and theoretical observation for these cross sections [25-27] and then to compare these results with the observed dependence of several sparsely populated data points to establish consistency. The second approach was to depend more heavily on the experimental observations and make a more detailed measurement of the asymmetry as a function of the mass of the spectrometer and then make the extrapolation to zero detector mass explicitly. It was the design of this experiment to acquire data with the mass of the spectrometer and decay volume scaled by factors of ~ 4 and ~ 8 in order to be able to extrapolate to zero mass with good accuracy.

One of the significant improvements of this spectrometer was its mass composition. This experiment was carefully designed to minimize presence of isotopically impure ($I \neq 0$) substances. To this end a level of free hydrogen of less than 18 mg/cm^2 was obtained, and an overall proton-neutron difference of 1 part in 10^3 was achieved (see Appendix 1 for details). Furthermore, in scaling the mass of the spectrometer to higher values, great pains were taken to do this as uniformly as possible while maintaining the isotopic balance. The placement of this extra material was made as close as possible to the existing mass concentrations, e.g., Čerenkov mirrors, proportional chambers, and hodoscope counters. The detailed placement of the initial mass is given in Table VII.

When taking this additional data during the experiment, special attention was given to the contribution of each measurement to the statistical error

on the extrapolated value at zero mass. In order to optimize the data acquisition, data were originally taken in the ratio of 3:2:1 for x1, x4, and x8 mass respectively with additional data being taken in the x8 mass configuration to study the effects of decreased isotopic impurities in the spectrometer constituents. Additional data were recorded to study specific effects of localization of material (e.g., Čerenkov mirrors, and decay volume) in the spectrometer. This approach to the major systematic problem, the effects of material on the asymmetry, makes the final result less sensitive to the detailed nature of this correction. In addition, this systematic treatment results in the ability to extrapolate out nearly all mass dependent effects present (e.g., neutron and K_L^o interactions in the spectrometer, delta ray production and πN scattering effects). Further discussion of the resulting analysis will be given in the following sections.

CHAPTER III

PRIMARY ANALYSIS

This experimental effort resulted in the collection of $\sim 10^8$ K_{e3} decay candidates which had to be analyzed individually with the analysis involving a full kinematic reconstruction. Thus a major task in the experiment was developing and carrying out the processing of this large quantity of data in a finite period of time while being further constrained to do all of this for a finite amount of money. Since one of the objects of this experiment was a thorough investigation of systematic and instrumental effects, it was realized that this scheme must retain enough flexibility to allow such an investigation.

The processing of the data was therefore conducted in three stages. First, a primary analysis of the raw data tapes was conducted; this step was designed primarily as a track-finding program with kinematical reconstruction of the decay. This step separated out from the raw data those events likely to be of interest and compressed all the kinematical and geometrical information into a compact form for each event and then wrote this information onto magnetic tape. Second, these new tapes were further analyzed and the results stored on tertiary tapes using programs which had the option of printing histograms if desired. Lastly, these tertiary tapes were formatted in such a way as to allow final inspection of the data (e.g., cuts) for a minimum cost in computation. The details of these major steps in the analysis follow.

A. Track Recognition and Reconstruction

The first stage of the analysis consisted of reconstructing tracks through the five chamber planes of the spectrometer from the information recorded on

magnetic tape. There were some features of the raw data which required special attention before the track finding was undertaken.

From a study of the initial bit patterns for events recorded on tape, it became apparent that there were considerably more adjacent channels triggered in the proportional chambers than expected on the basis of random noise in the electronics. This effect was observed to be caused by particles passing through the small region between neighboring channels and firing the discriminators for both channels. Therefore, when adjacent channels were found "on" the extra position information was exploited and the position of the particles was taken as the average of the two channels.

The other characteristic of the proportional chambers which had to be confronted was the effect of detection of "induced pulses" by the chamber electronics. These "induced pulses" were first observed by Charpak et al.[20] in their studies of the characteristics of multiwire proportional chambers. These "induced pulses" originate from the electrostatic properties of the proportional pulse propogation in the chambers. In addition to the negative electron pulse which moves in toward the signal wires, there is a positive induced charge which is distributed among neighboring wires (both signal and high voltage). These positive pulses are also sensed by the differential amplifiers used to detect the normal proportional signals. As a result of this property of the proportional chamber and the particular arrangement used, when multiplication occurred at the edge of one chamber element , 2 pulses would appear in the chamber, one in the originally struck channel and another in a channel once removed to the right or left depending on the original channel struck. Since this effect was present only under these very restrictive geometrical conditions, this characteristic could be used to further improve the spatial resolution of the chambers.

In order to account for this effect in the chambers, the software of the reconstruction program was designed to remove these "induced" signals by using a simple algorithm which was determined by the configuration of the electronics (see Fig. 4).

The remaining modified bit pattern was then converted into a set of horizontal position coordinates for each event. This association was easily carried out, since the initial surveying of the chambers located them in space to within ± 1/32 inch in both the horizontal and vertical directions. The data was transformed into a set of common coordinates with the beam defining the positive Z direction and with the center of the spectrometer magnet being at coordinates (0,0,0). The positive X coordinate axis was taken to be the plane of the horizontal and to the left of the beam as one faces downstream, and positive Y axis taken to be in the vertical direction. The points in the chambers were taken a pair at a time from a given side in the back chambers with the program saving the points and the value of the projection of the ray to the center line plane of the spectrometer magnet (Z = 0). Then front track segments were formed using both two and three point segments on a given side of the apparatus and a match was looked for with "any" of the back tracks that fell within a given window at the center-line plane of the spectrometer magnet. The size of this window had three values depending on the front chambers involved in the event. This window size was independent of the magnet center line intersection point and was a constant for a given set of front chambers involved (see Appendix 2). The program looked for as many as four full tracks in the spectrometer with the condition that no more than 2 were on a given side of the apparatus upstream of the magnet. Once a set of tracks had been found and a Čerenkov cell was recorded as being "on", the event was further processed to investigate in detail its kinematical

properties. The quantities that were calculated and saved were; decay vertex, momenta of secondaries, M^* of πe system, and center-line intersection points for both tracks. Nearly 90% of the raw data was retained at this stage of the program.

The momenta of the secondaries were determined by fitting to two intersecting straight lines constrained to meet at (Z = 0) to the points of a given track found in the spectrometer. The slopes of these curves were then used to evaluate the projection of the bending angle in the horizontal plane of the spectrometer. As a result of the geometry of the magnetic field of the spectrometer magnet the "square field" approximation could be used to evaluate the momenta of the secondaries. This resulted in a measure of the projected momenta in the XZ plane of

$$p_{XZ} = \frac{e\, B_o\, L_{eff}}{\sin\theta_{in} - \sin\theta_{out}} \quad . \qquad \text{(III.1)}$$

When operating the magnet with a central field of 4.92 kG. an overall momentum transfer of 116 MeV/c to each secondary particle resulted. These momenta were of interest when making the mass correction for the data as a function of pion momentum, which allows isolation of specific regions of rapid flucuations in the πN cross sections, or in investigating possible differences in the measured asymmetry due to other physical phenomena or systematic effects. To maximize the efficiency of information storage, a binning scheme was implemented which facilitated the study of these effects at later levels of analysis without any loss in information content.

B. Event Quality Categories

In addition to the data previously described, the primary analysis program

also generated information for each event which rated its quality based on certain reconstruction parameters and other geometrical information. Along the same lines, several classes of events were established to isolate data which suggested possible enhancements of accidental K_{e3} triggers. The tests performed to establish these categories were as follows:

(1) Was there a track that passed through the appropriately flagged Čerenkov element? If not, these events were tagged "Čerenkov inconsistencies".

(2) Were both tracks found consistent with their respective intersections with the tagged rear hodoscope elements? If one or both tracks were inconsistent, the event was flagged as being a "hodoscope inconsistency".

(3) In the cases where there were more than one front (back) track segments matching a back (front) segment within the allowed windows, the pair which had the best match was chosen for reconstruction purposes and the event was then flagged as having had "greater than one track" present.

(4) If both tracks in the spectrometer had charges determined to be of the same sign, these events were flagged as "similar bending". This check was made assuming perfect angular resolution and was refined at a later stage to reflect the confidence limits involved in saying that both particles were measured to have the same sign.

(5) Having allowed the reconstruction program to find as many as 2 full tracks on a given side of the spectrometer, the question was asked whether there was any disagreement as to the sign of the secondary particle for these tracks. If the two tracks on the same side of the spectrometer implied a different charge for the secondary particle, the event was flagged as "ambiguous". All ambiguous tracks were by definition events also classified as "greater than one track" events.

(6) A χ^2 was computed for the fit of the four (or five) points of the tracks found in the chambers, to the two intersecting line segments that were found for each track using a least square fitting procedure. This χ^2 was stored for future reference.

(7) The number of missing chambers in the front of the spectrometer was preserved since, as was pointed out earlier, this makes a substantial difference in the "matching" criterion for a reconstructed event. In addition it can supply information concerning the dependence of the measured asymmetry on chamber inefficiencies.

A breakdown of the data, including these event categories, is shown in Table VIII. This secondary data information was then formatted into 2 (32 bit) words and was written out for each event for which agreement with K_{e3} signature was satisfied. By undertaking this analysis the original sample of 500 (7 track, 556 BPI) magnetic tapes were transformed into 25 (9 track, 1600 BPI) data tapes which improved the logistics involved in analysis by a factor of $\sim$ 20, and did so without any great loss of input information.

The burden of this primary analysis was divided roughly in half between the Princeton University Computer Center's IBM 360/91 and the group's own Hewlett-Packard 2116B 16K mini-computer. The 360/91 would process a primary event in .2 msec which meant a total of $\sim$ 40 hours CPU time for half the primary analysis, while the Hewlett-Packard, computing slower but a bit more dependably, would process an event in 30 msec resulting in roughly one month of 24 hour running. The use of the small computer resulted in a substantial saving in computation costs for this stage of the analysis ($10K). However, since the Hewlett-Packard machine is much smaller than the 360/91 some modification to the form of the analysis was necessary. This aspect of the analysis was checked thoroughly, and the final

results were observed to be independent of which machine performed the analysis.

C. Further Data Analysis

The next two steps of the analysis procedure were designed to organize the data in such a way as to facilitate thorough investigation using a minimum amount of computer time. The essential aspects of these next two phases were flexible enough to allow several separate reductions of the data under various general conditions.

The final form of the data was a 32768-element array whose dimensions represented various bins for the data (e.g., electron charge, momenta of secondaries, vertex position, center line crossing, c.m.s. energies, and event quality). By summing over the data and constructing such an array one could very easily perform cuts on all of the data and check the effect of such cuts. The stage of analysis preceeding the formation of these final arrays was arranged to eliminate repetition of any calculation on the data. The results of this stage of the analysis will be covered in the next chapter.

CHAPTER IV

DATA REDUCTION

After the kinematical reconstruction, the data were subjected to various cuts in order to select the sample which was freest from systematic biases and backgrounds. In addition, several categories of events which were likely to be enriched sources of background events were studied in order to estimate the corrections due to background contamination. In the sections that follow the cuts and corrections will be described in detail and a fully corrected value of the charge asymmetry will be obtained.

A. Initial Cuts

There were several cuts made on the data which were dictated by the experimental arrangement and the inherent resolution of the spectrometer. These initial cuts were:

(1) A fiducial volume cut was made on the allowable decay vertices. This cut restricted the origin of the decay to be at least 14 inches downstream of the beam anticounter and upstream of chamber 2 ($-72" > Z > -191"$). A cut was also made on the horizontal vertex position (X), requiring events to have originated within ±3 inches of the beam axis. Events whose horizontal vertex position was outside this range were expected to be primarily accidentals and will be discussed separately.

(2) A minimum bending angle requirement was set at 50 mrad (corresponding to a momentum of 2320 MeV/c) for each track. This value was determined by measurements made on the angular resolution of the spectrometer using magnet-off

data. This cut-off was necessary in order to insure unambiguous determination of the charges of the secondaries.

In addition, a low momentum cut-off was imposed to eliminate background events (200 MeV/c for electrons and 500 MeV/c for pions).

(3) In order to isolate events in which confusion might have arisen due to the windows necessary for track finding, a cut was imposed which required both tracks to cross the center line of the magnet at a distance greater than 6. inches from the beam center line. This cut also served to remove beam associated backgrounds which might be present.

(4) All events for which an anticounter was tagged were removed. In addition, events which were classified as similar bending, ambiguous, Čerenkov inconsistencies, and hodoscope inconsistencies were removed (for details, see Chapter III.).

The contribution of each of the above categories to the data sample is shown in Table VIII. The data surviving these cuts were then subjected to a detailed systematic analysis.

B. Internal Consistency Checks

There were three separate tests performed on the data in this investigation. The first test was to verify the linear dependence of the charge asymmetry with spectrometer mass in order to make the extrapolation to zero mass. The second test used Monte Carlo techniques to simulate K_{e3} decays as a limited verification of the detector's sensitivity to this decay mode. The third and final test required the results to be stable under the applied cuts, and further to yield consistent results for various subsets of the data considered. Each of

these aspects of the analysis is discussed below.

(1) Mass Dependence of the Asymmetry

This aspect of the experiment was carefully designed to enable an extrapolation for nearly all mass dependent effects in the detector and the decay volume. In addition to the direct measurement of the mass effects an estimate of its magnitude was made. The effects included were positron annihilation, $\pi^+\pi^-$ differential absorption, neutron and K_L^o interactions, and delta ray production. This calculation appears in Appendix 1 and results in an estimated correction of

$$\Delta\delta_{calculated} = (+.35)*10^{-3} \quad \text{per } .637 \text{ g/cm}^2 \quad .$$

The result of the mass extrapolation was

$$\Delta\delta_{measured} = (+.54 \pm .13)*10^{-3} \quad \text{per } .637 \text{ g/cm}^2 \quad .$$

The agreement of these results is satisfactory in view of the approximations involved in this estimate. The behavior of the data as a function of spectrometer mass for the initial cuts is shown in Fig. 7.

(2) The Comparison of Data and Monte Carlo Calculation

The function of this calculation was primarily as a diagnostic tool in investigating systematic effects. However it also provided some information regarding the consistency of the data with the kinematics of K_{e3} decay, which was used to locate possible sources of background contamination.

To generate this data the standard V-A weak interaction for K_{e3} decay was assumed[28] viz.,

$$M \sim \bar{u}_e \gamma_\mu (1 + \gamma_5) u_\nu \{f_+(q^2) (p_K + p_\pi)_\mu + f_-(q^2) (p_K - p_\pi)_\mu\}. \quad \text{(IV.1)}$$

For K_{e3} decays the quantity $(p_K - p_\pi)_\mu \sim m_e$ and can be neglected. The form of $f_+(q^2)$ was

$$f_+(q^2) = f_+(0)\{1 + \lambda_+ (\frac{q}{m_\pi})^2\} \quad \text{(IV.2)}$$

with

$$\lambda_+ = .024 \quad .$$

The results of the calculation were relatively independent of the value of λ_+ thereby decoupling this result from the present experimental disagreement[29-32] as to the value of this parameter.

The data were generated being weighted by the above Dalitz plot density, beam distributions, and kaon momentum spectrum. The events which were accepted by the apparatus were recorded on magnetic tape in a format similar to that of the primary data tape. Processing this data with the primary and secondary analysis programs served to test the programs for errors and to check the data for inconsistencies with the calculations. Some comparisons of data and Monte Carlo are shown in Figs. 8, 9.

From these calculations the apparatus' acceptance was measured to be $\sim$.6% for K_{e3} decays. With this acceptance and the observed event rates during data taking of $\sim$ 65 events/10^{12} protons on target, an estimate of the neutral kaon flux in this beam is $\sim 3 * 10^4$ $K_L^o/10^{12}$ protons on target. The Monte Carlo data was further used to evaluate other systematic effects and biases in the spectrometer. A discussion of these results appears in a later section.

(3) Internal Consistency of the Data

One of the useful properties of the data was the presence of two distinct event topologies (see Fig. 10). These topologies were characterized by the sense of their deflection in the spectrometer, and were named appropriately "inbending" and "outbending". These two distinct classes of events provided an additional degree of symmetry which was extremely helpful in isolating problems in the data.

In separating the data into these two topological categories an inconsistency in the extrapolated asymmetry emerged. The difference in the extrapolated charge asymmetry for these two categories was

$$\delta_{\text{inbending}} - \delta_{\text{outbending}} = (1.64 \pm .53)*10^{-3}$$

with no observed difference in the slopes of the mass extrapolation. In searching for correlations of this effect with reconstruction difficulties, geometry, and/or backgrounds this difference was observed to be concentrated in the decay region for -72 inches < Z < -105 inches (Fig. 11). No further correlations with momenta of the secondaries, reconstruction difficulties (e.g., cuts made on χ^2 of tracks or cuts made on "greater than one track" events), front chamber inefficiency or beam associated backgrounds were observed.

Requiring the results of the extrapolation to be independent of the two topologies imposed a stringent cut on the vertex position. After making this cut on the data (i.e., -105 inches > Z > -150 inches, see Table IX) and performing the mass extrapolation, the following charge asymmetry was obtained,

$$\delta = (2.53 \pm .34)*10^{-3} \quad .$$

This cut on the vertex did not effect the linearity of the asymmetry as a function of mass. This is illustrated in Fig. 12.

C. Evaluation of Systematic Effects

The observation of the difference in asymmetries in the two event categories for the total sample of data precipitated a detailed investigation of several aspects of the experiment. No single effect satisfactorily explained the difference. A description of these and other systematic effects that were checked for follow.

(1) A re-examination of the analysis programs uncovered no problems which could result in misidentification of the topology of an event. This was further verified by analyzing 100K Monte Carlo events and finding complete consistency between the generated and analyzed topologies.

(2) A search for any polarity dependent change in detection efficiency for each of the elements in the spectrometer was carried out. The data presented in Fig. 11 were suggestive, indicating evidence perhaps of a systematic effect which was contributing a positive excess to the inbending events and a negative excess to the outbending events. In taking an average over the extrapolated asymmetries for inbending and outbending data as a function of Z vertex position, which weights both sets of data equally, such a systematic bias should cancel. The result of this averaging is shown in Fig. 13. Although the data seems to be consistent with such an argument, all searches for such effects in the apparatus indicated no serious difficulty. In a study of the rates in all the chamber and counter elements from the primary data tapes, an upper bound to effects on the charge asymmetry due to changes in detection efficiency was

$$\Delta\delta \sim 10^{-5} \quad .$$

The Čerenkov counter deserves special attention with regard to these arguments since it had a $\sim$ 100% differential sensitivity for electrons and pions. A change in the performance of this counter with polarity could contribute directly to a first order change in the measured asymmetry (Appendix 3). The first check of the Čerenkov counter was a look at the extrapolated charge asymmetry measured for each of the four phototubes. The result of this separation showed the asymmetry of each Čerenkov tube to be consistent with that of the total sample of data, thus verifying the absence of any effects due to differential performance of the phototubes. This result is especially encouraging since isolating the data in this manner results in an increased sensitivity to apparatus biases.

In a second study the pulse height spectrum of each of the Čerenkov elements was studied. The observed pulse height spectra were consistent with the detection of 6 photoelectrons/K_{e3} decay electron. This photoelectron level was

stable to 10^{-2} for the two polarity settings for all elements of the counter. Using Poisson statistics to describe the photoelectron distribution in the counter, the efficiency of the i^{th} cell is

$$\varepsilon_i = \sum_{n=\text{threshold}_i} P_{\lambda_i}(n)$$

where

$$P_{\lambda_i}(n) = \frac{\lambda_i \, e^{-\lambda_i} \, n}{n!} \quad .$$

Setting the threshold at one photoelectron, a change in the average number of photoelectrons detected with polarity then results in a change in efficiency of

$$\Delta\varepsilon_i = \sum_{n=1} P_{\lambda_i^A}(n) - P_{\lambda_i^B}(n)$$

which for small changes

$$|\lambda_i^A - \lambda_i^B| \ll 1$$

becomes,

$$= P_{\lambda_i}(0) * (\lambda_i^A - \lambda_i^B) \quad .$$

For the numbers given above, this results in a change in efficiency of 10^{-5} which is negligible.

(3) The inbending/outbending difference was not localized in time or to any specific spectrometer mass configuration during the experiment. Looking at this difference on a tape by tape basis for the x1 mass data a difference of $(1.95 \pm .61 * 10^{-3})$ results, with a χ^2 for the data of 302 for 283 degrees of freedom. These data are presented in Fig. 14.

(4) The effects of the fringe field of the spectrometer magnet on the performance of the proportional chambers was investigated. It was thought that there might arise a differential aperturing effect due to dispersion of proportional pulses near the edges of the chamber's active regions which would be sensitive to magnet polarity reversals. The symmetry of the proportional chamber

field about the signal plane, however, causes the effect to cancel out as a function of magnet polarity. In addition, the charge asymmetry was studied as a function of the position of the pair of tracks in the front chambers, with the conclusion that there was no measurable aperturing taking place.

(5) Since the earth's magnetic field is non-reversible, it can introduce a differential effect in the acceptance of events as a function of the spectrometer magnet polarity. Using various estimates of the average track length and the magnetic field strength of the earth in the spectrometer, results in a shift in the momenta of the secondaries by 1 part in 10^4. To test the sensitivity of the apparatus to such small shifts in momenta, the Monte Carlo data were used. Two samples of data were generated with a difference in magnetic field an order of magnitude larger than those calculated. The result of this showed no differential treatment of inbending and outbending data large enough to be a problem. In addition the localization of the difference in the downstream end of the decay volume makes the arguments for such effects even more untenable.

(6) A further possibility that the difference in these asymmetries could arise from delta ray production in the Čerenkov mirrors which in turn are reflected back into the counter by the fringe fields of the spectrometer magnet resulting in detection of the electron, was considered. Since only knock-on electrons can be produced, this type of event results in a large difference in asymmetry for the two event topologies. A calculation was made using Monte Carlo data to evaluate this effect and is described in detail in Appendix 1. The results of this study showed the effect to be much too small to produce the observed behavior in the two event topologies. In addition this effect should extrapolate out with the mass of the spectrometer making the effect even more unlikely.

In summary no workable explanation of the differences in the asymmetries has yet been devised. This does not, however, result in any unresolvable difficulties. The added symmetry of the results for the two topological categories clearly indicates the region of difficulty. Having this extra constraint on the data has been indispensible in establishing a result which is free from systematic biases.

D. Corrections to the Data for Backgrounds and Accidentals

To conclude the discussion of the results, corrections must be made on the final sample of data for the various background and accidentals present which were not dependent on the mass of the detector. To make these corrections the several categories of data, presumed rich in accidental events, were used. By investigating the charge asymmetry of these event classes, corrections to the final data can be made. The corrections were the following:

(1) Vertex Failures

Events for which the horizontal vertex position was > ±3 inches from the beam were expected to represent an enhanced source of background events. The extrapolated asymmetry measured for these events was

$$\delta_{\text{X failure}} = (-13.20 \pm 4.16)*10^{-3},$$

with no difference in asymmetry for the two event topologies. The level of these accidentals present under the beam profile was determined by the horizontal vertex (X) distribution of the data and the events which had identical charge secondaries (similar). These data indicate a level of $\leq .5\%$ contamination, which results in a correction to the data of

$$\Delta\delta \leq (+.07 \pm .021)*10^{-3}.$$

(2) Čerenkov Inconsistencies

Events of this type could have resulted from knock-on electrons

produced by the mechanism previously described. However, since this effect was dependent on the mass of the spectrometer, it is eliminated by the mass extrapolation procedure and will not be considered here. The remaining possibility, which does not depend on the mass of the spectrometer, is that a Čerenkov tube accidentally triggered in coincidence with two tracks in the spectrometer generating an acceptable event signature. The asymmetry of this data was

$$\delta_{\check{C}erenkov\ inconsistency} = (-2.57 \pm 2.70)*10^{-3} \quad .$$

These events comprise $\sim$ 1% of the final cut data. Associating the rates of accidentals with the rate of tracks through the counter, where the rates in the elements nearest the beam are twice those of the two outer elements, a contamination of $\sim$ 1.2% results. Using this number of events the correction to the data becomes

$$\Delta\delta \simeq (+3.2 \pm 3.4)*10^{-5} \quad .$$

(3) Hodoscope Inconsistencies

These events have a measured asymmetry of

$$\delta_{Hodoscope\ inconsistency} = (-8.0 \pm 5.1)*10^{-3} \quad ,$$

with this class of events representing approximately .3% of the data. The frequency distribution of back hodoscope tags for the data showed a nearly uniform distribution in all 4 elements of each bank. If these events originated from solely accidental tags the effective level of contamination decreases by a factor of 4, resulting in a contribution to the change in charge asymmetry of

$$\Delta\delta = (+0.6 \pm 0.3)*10^{-5} \quad .$$

(4) Similar Bending Events

This class of events, if associated with events with 2 bona fide tracks in coincidence in the spectrometer, indicates the level of a background contamination in the data. However, it was also possible, in spite of the bending angle

requirement placed on the data (i.e., > 50 mrad), for events to be reconstructed in such a way as to have their topologies appear to change. Calculating the probability of a single track that is inbending being reconstructed as a track that is outbending, thereby making a similar event, nearly 80% of the similar curvature events can be accounted for.

The asymmetry of these events was measured to be

$$\delta_{Similar} = (0.36 \pm 3.87)*10^{-3}$$

with a contribution to the data of $\sim$ 1% before the previous calculation was taken into account. An upper limit to the change in the asymmetry for these events is

$$\Delta\delta \leq (+.4 \pm 3.9)*10^{-5} \quad .$$

(5) Inefficient Anticounters

The discussion of anticounter inefficiencies is separated into two parts; the decay region anticounter and the magnet aperture anticounters. The asymmetry measured for these two categories was

$$\delta_{Beam\ anti} = (-5.00 \pm 1.3)*10^{-3}$$

$$\delta_{Magnet\ anti} = (-2.90 \pm .75)*10^{-3}$$

with no evidence of in-outbending difference.

To evaluate the possible effects of each of these groups on the total data one must fold-in the inefficiency of each of the anti systems. For the decay region anticounter a measurement of its tagging efficiency during data taking showed an efficiency of > 99.5% with the rate of events with and without this counter tagged of 1:3. This .5% inefficiency results in a correction to the asymmetry of

$$\Delta\delta = (+8. \pm 2.0)*10^{-6}.$$

In addition during the experiment several million triggers were recorded with this anticounter out of the logic for K_{e3} trigger but still tagged in order

to get an enriched sample of these events for later study. The asymmetry of this data as a function of vertex position showed this data to be in agreement with the cut data, thus discounting any serious problem due to this class of events on the final result.

The contamination of the data by inefficient magnet anticounters was very much the same. A measurement of the efficiency of these counters shows them to be < 1% inefficient during the running of the experiment where approximately 12% of the data were in this category. This inefficiency results in a correction to the data of

$$\Delta\delta = (+3. \pm .75)*10^{-6} \quad .$$

(6) Regeneration and Other K_L^o Interactions Upstream of the Detector

These two effects when originating from interactions upstream of the decay volume or at anti (E) represent a source of background which does not extrapolate out with the other mass effects. Here an estimate is made of the level of this uncorrected source of background.

First the effect of regeneration of K_S^o by interactions of the beam with the last collimator and the anticounter (E) can be shown to be insignificant. The regeneration amplitude (ρ) for copper was measured in a previous experiment (19) in this beam with the result of $\rho = .10$ for 9-1/8 inches of copper. Using this as an estimate of the effect of K_L^o's scraping the last collimator, a correction to the data of

$$\Delta\delta \lesssim (+10^{-8})$$

results. This number reflects the effects of apparatus acceptance near the anticounter ($\sim 10^{-2}$), the regeneration of K_S^o ($\sim 10^{-2}$), the survival rate of K_S^o to the decay volume ($\sim 10^{-2}$), and the asymmetry after a regenerator ($\sim +10^{-2}$).

As for the interactions of K_L^o in the collimators and the anticounters producing Λ^ohyperons which have a charge asymmetry of -1, the same types of arguments

hold. Despite the large charge asymmetry, the number of Λ^o's produced and surviving to the decay volume result in a correction to the charge asymmetry of

$$\Delta\delta << (\pm 10^{-7}) ,$$

which is also negligible.

E. Summary of Results

The charge asymmetry for the final sample of cut data after the extrapolation to zero mass is

$$\delta = (2.53 \pm .34)*10^{-3} .$$

The remaining systematic corrections to this result are:

X-vertex failures	$(+.07 \pm .021)*10^{-3}$
Čerenkov inconsistencies	$(+.032 \pm .034)$
Hodoscope inconsistencies	$(+.006 \pm .003)$
Similars	$(+.004 \pm .039)$
Inefficient anticounters	$(+.011 \pm .002)$
Regeneration	$(+.0 \pm \quad)$
	$(+.123 \pm .052)*10^{-3}$

When these corrections are included, the final value of the asymmetry becomes

$$\delta = (2.66 \pm .34)*10^{-3} .$$

CHAPTER V

CONCLUSIONS

The charge asymmetry for $K_L^o \to \pi^{\pm} e^{\mp} \nu$ in this experiment is

$$\delta_{K_{e3}} = (2.66 \pm .34)*10^{-3} \quad .$$

It is of interest to compare this result to those of other experiments on the K system via Equations (I.14) and (I.21).

The present experimental status of these CP violating parameters was discussed in a recent review by V. Fitch [33]. From this paper one gets the following values for the parameters of interest in relating the charge asymmetry measurement to other independently measured quantities.

$$|\eta_{+-}| = (1.95 \pm 0.03)*10^{-3}$$

$$\Phi_{+-} = (42.4 \pm 2.3)^o$$

$$|\eta_{oo}| = (2.08 \pm 0.16)*10^{-3}$$

$$\Phi_{oo} = (43. \pm 19.)^o$$

$$\mathrm{Rex} = 0.05 \pm {}^{0.25}_{0.35}$$

$$\mathrm{Imx} = -0.01 \pm 0.02$$

These experimental results coupled with the phenomenological description of Wu and Yang outlined in Chapter I, were then used to place an upper limit on ε', i.e.,

$$\mathrm{Re}\varepsilon' = -0.03 \pm {}^{.18}_{.13}$$

$$\mathrm{Im}\varepsilon' = -0.03 \pm {}^{.66}_{.13} \quad .$$

The Wu-Yang triangle thus becomes the Wu-Yang line. Using these experimental results for η_{+-}, η_{oo}, and x one predicts the charge asymmetry to be

$$\delta = 2\mathrm{Re}\varepsilon = 2|\eta_{+-}| \cos\Phi_{+-}$$

$$= (2.90 \pm 0.17)*10^{-3} \quad .$$

If one compares this result with the world average for the charge asymmetry in K_{e3} decays which includes this result

$$\overline{\delta}_{Ke3} = (2.83 \pm .20)*10^{-3}$$

one sees that they are in extremely good agreement. This close agreement makes it clear that the representation of Wu and Yang is adequate to the present limit of experimental accuracy.

Another aspect of the charge asymmetry measurement which should be mentioned is the consistency between the asymmetries measured in K_{e3} and $K_{\mu 3}$. The average asymmetry for the $K_{\mu 3}$ measurements [10, 11] is

$$\overline{\delta}_{K\mu 3} = (2.79 \pm .81)*10^{-3} \quad .$$

This number is also in agreement with the above K_{e3} value, however, this comparison is relatively meaningless at the present level of statistical power in the $K_{\mu 3}$ results.

At the outset it was pointed out that this asymmetry measurement was also sensitive to a new source of CP violation as described by Bell and Zia [5] and independently by Brodine [6]. In the process of evaluating the sensitivity of this experiment to these final-state interactions a taste of several of the difficulties attendant on this effect was noted. As an example of these difficulties a calculation was made of the effects of the differential $\pi^{\pm}N$ scattering on the Dalitz population. This calculation showed that there were significant numbers of events which got shifted in a charge asymmetric way thereby producing a variation of the asymmetry across the Dalitz plot which was comparable to the size of these final-state interaction effects. As a result it would appear that future high precision experiments aimed at studying this effect must place a high premium on reducing the detector mass still further.

In summary, the questions regarding the origin of CP violation in the K^o-$\overline{K}^o$

system are still open. The present level of accuracy in experimental results has served to eliminate very few of the proposed theoretical explanations of this effect. At present there are still several theories which are consistent with the data and none of which seem to deserve any special consideration as being more likely than any other (see Ref. 33). The theories that have been eliminated from consideration are: the theory which has the source of CP violation originating from $\Delta I = 5/2$ transition which requires $\eta_{oo}/\eta_{+-} \simeq 2$, and less definitely, the weak-e.m. theory of CP violation which is put on uncomfortable ground due to the present status of the measurement of the neutron dipole moment. It is quite clear that the level of experimental sensitivity must be improved by 1 or 2 orders of magnitude in order to test the remaining theories to the level where the situation can be more explicitly delineated.

ACKNOWLEDGEMENTS

As in any experimental effort of this magnitude there are many people who have contributed to its overall success. The involvement of the four collaborators V. Fitch, V. Hepp, D. Jensen, and M. Strovink formed the foundation of this effort. The leadership of Prof. V. Fitch provided an especially sound environment for the scientific development of his students. The experience and enthusiasm of Drs. Jensen, Strovink, and Hepp were indispensible during the data taking phase of the experiment.

During the data analysis, all of these collaborators had many useful suggestions to make regarding the handling of this data which were extremely useful in later stages of analysis. Especially helpful in this aspect of the experiment were Mr. V. Bearg and Ms. A. David. Mr. Bearg provided the necessary link between the complexities of the physicist's mind and the complexities of a sometimes cooperative computer. Ms. David had the unenviable task of implementing several stages of the analysis of this data, thus making life a bit more bearable for a certain graduate student. In addition Ms. David is also responsible for the typing of this manuscript, an effort for which the author is personally extremely thankful.

This experiment also owes a great deal of its success to the vigorous support of the Elementary Particles Laboratory of Princeton University. The professional competence and technical support of this facility has contributed immensely to the success of this endeavor. It is also important to recognize the help and cooperation of the operating crew of the AGS that made much of this possible, by providing the necessary support and $\sim 10^{18}$ 28 GeV protons that were needed to accomplish the data taking.

The author also owes thanks to two fellow graduate students for their contributions to the success of this experiment. Mr. Y. Fukushima was extremely helpful during the setting up of this experiment and Ms. R. M. Baltrusaitis was also appreciated for her help with the Monte Carlo calculations.

Finally the author owes special thanks to his wife Patricia and his children Robert and Suzanne for their encouragement and patience throughout this endeavor.

APPENDIX 1

CALCULATION OF EFFECTS OF MATERIAL ON THE MEASUREMENT OF THE K_{e3} CHARGE ASYMMETRY

As has been pointed out previously the presence of mass in the detector and decay volume can induce a charge asymmetry from a number of effects. Among the most predominant are positron annihilation, differences in the π^+ and π^- absorption and scattering, production of background through the interactions of K_L^o's and neutrons in the decay volume, and the production of knock-on electrons by one of the decay products from other K_L^o decay modes which are subsequently detected in the Čerenkov counter.

Each of these effects is removed by the extrapolation to zero mass in the detector and decay volume. It is of interest, however, to attempt to estimate the magnitudes of these various effects and compare the results of these calculations with the measured value.

A. e^+e^- Annihilation

The cross section for positrons of energy E annihilating on electrons at rest in material can be expressed as (e.g., see Ref. 34)

$$\sigma_{e^+e^-} = \left(\frac{3/8\ \sigma_{TH}}{\gamma^2 - 1}\right)\left((\gamma + 4 + \frac{1}{\gamma})\ \ln(\gamma + \sqrt{\gamma^2 - 1}) - \sqrt{\frac{\gamma - 1}{\gamma}}(\gamma + 3)\right) \quad \text{(A1.1)}$$

which in the limit of $\gamma >> 1$ becomes

$$\sigma_{e^+e^-} = 3/8\ \sigma_{TH}\left(\frac{\ln(2\gamma)}{\gamma}\right) \quad \text{(A1.2)}$$

where σ_{TH} is the Thompson cross section (665 mbarns), and $\gamma = E/m_e$. In order to

evaluate the change in the measured asymmetry due to this annihilation process this cross section must be averaged over the observed K_{e3} secondary electron momentum spectrum as well as averaging over the atomic charge (Z) of the various spectrometer constituents. The average over the momentum spectrum yields an effective cross section of

$$\overline{\sigma_{e^+e^-}} = (1.41 \pm .007) \text{ mbarns/electron} \quad .$$

Further averaging over the spectrometer constituents ($\overline{Z} = 8$ and $\overline{A} = 16$) one arrives at the probability of a positron annihilating in the spectrometer at the minimum mass of .637 g/cm^2 of,

$$\Phi_{e^+e^-} = \frac{\overline{Z}\,\overline{\sigma}_{e^+e^-}}{\overline{A}} N_A \ (.637 \text{ g/cm}^2)$$
$$= (3. \pm .015)*10^{-4} \quad . \qquad \text{(A1.3)}$$

This differential absorption shifts the measured charge asymmetry by

$$\delta_{\text{Observed}} = \frac{N^+ - N^-}{N^+ + N^-} = \frac{N^+(1 - \Phi) - N^-}{N^+ + N^-}$$
$$= \delta_{+-\text{ true}} - \frac{\Phi}{2} \quad .$$

Based on these estimates the correction to the charge asymmetry is

$$\Delta\delta = (+.15 \pm .0007)*10^{-3} \quad \text{per .637 g/cm}^2$$

B. Differential $\pi^+\pi^-$ Interactions

In calculating these differential effects there are two basic types of interactions involved. For isotopically impure material there is the difference in the total $\pi^+\pi^-$ cross sections to be averaged. For the case of isotopically pure nuclei an effect results from the combined nuclear and Coulomb interactions.

A completely satisfactory treatment of this latter effect has never been achieved. To make an estimate of these effects a simplified approach was adopted [35].

First, since with charge independence the $\pi^+p(n)$ interaction is identical to $\pi^-n(p)$ interaction, it becomes quite clear why one strives for an isotopically pure detector. In this detector there were 18 mg/cm^2 of excess protons (hydrogen) and 6 mg/cm^2 of excess neutrons (from fluorine, chlorine, and argon). Since these neutrons are partially shielded by other nucleons in the nucleus, the effective amount of neutrons is diminished by about 1/3 resulting in a net proton excess of 14 mg/cm^2. Averaging πp cross sections [36] over the pion spectrum for these decays results in an average difference in $\pi^+\pi^-$ cross sections per proton of

$$\overline{\sigma_{\pi^+-\pi^-}} = (7 \pm .04) \text{ mbarns/proton} .$$

Using this difference in cross sections and equation (A1.3) one gets a probability of differential absorption of

$$\Phi_{\pi^+\pi^-} = (.59 \pm .0030)*10^{-4}$$

which yields a correction to the charge asymmetry of

$$\Delta\delta = (+.3 \pm .0015)*10^{-4} \quad \text{per 14 mg/cm}^2 \text{ of hydrogen.}$$

Next the differential absorption and scattering in the remaining isotopically pure material due to the differential Coulomb interaction between the nucleus and the $\pi^+\pi^-$ mesons must be considered. From classical considerations one can calculate the change in impact parameter for a given nucleus, charge Z, by a pion, momentum p and Compton wavelength $\lambda\!\!\!^{-}_{\pi}$,

$$\Delta R = \frac{Z \alpha \lambda\!\!\!^{-}_{\pi}}{\beta(p_c/m_\pi c^2)} . \qquad \text{(A1.4)}$$

If one characterizes the absorption cross section for these nuclei as

$$\sigma_a = \kappa \pi R^2 \qquad \text{(A1.5)}$$

where κ is ~ 0.7 for the nuclei of interest, this Coulomb effect results

in a change in the cross section of

$$\Delta\sigma_a = 2\kappa\,\pi\,R\Delta R \quad .$$

Evaluating this leads to a change in the measured charge asymmetry of

$$\Delta\delta = -\kappa\,2\pi\,\frac{R\,Z\alpha\,\lambda\!\!\!^{-}_{\pi}}{\beta(pc/m_\pi c^2)}\,N_A \quad \text{per 1 g/cm}^2 \quad , \qquad \text{(A1.6)}$$

for material with an average $\bar{Z} = 8$, R = 3.9f, p = 840 MeV/c gives a

$$\Delta\delta = (.9 \pm .004)*10^{-4} \quad \text{per .637 g/cm}^2 \quad .$$

Lastly the effects of the interference between the nuclear and Coulomb amplitudes will be discussed. The real part of the Coulomb amplitude for an extended nucleus is (e.g., see Ref. 37)

$$\mathrm{Re}(f_C(\theta)) = \frac{-2Z\,\alpha\,\lambda\!\!\!^{-}_{\pi}}{(p/m_\pi)\theta^2}\,g = \frac{-2Z\,\alpha\,\lambda\!\!\!^{-}_{\pi}}{(p/m_\pi)\theta^2}\,e^{-\theta^2/4\theta_o^2} \qquad \text{(A1.7)}$$

where g is the nuclear form factor which can be represented by $e^{-\theta^2/4\theta_o^2}$. The imaginary part of the Coulomb amplitude is not included since it does not change sign with the sign of the incident particle.

The nuclear amplitude is parameterized as

$$\begin{aligned} f_N(\theta) &= f_{Re}(\theta) + i f_{Im}(\theta) \\ &= (\alpha(\theta) + i)\, f_{Im}(\theta) \end{aligned} \qquad \text{(A1.8)}$$

with $\alpha(\theta)$ being the ratio of real to imaginary parts of this amplitude for a given angle θ. It is assumed that $\alpha(\theta) = \alpha(0)$. The value of $\alpha(0)$ is known for pion nucleon scattering from the application of dispersion relations. These factors for nuclei are obtained by using an optical model calculation which yields

$$\alpha_N(0) = \frac{\mathrm{Re}\,\frac{f(0)}{k}}{\mathrm{Im}\,\frac{f(0)}{k}} = \frac{e^{-\sigma_T N\ell}\,\sin\frac{\alpha(0)\sigma_T N\ell}{2}}{(1-e^{-\sigma_T N\ell})\,\cos\frac{\alpha(0)\sigma_T N\ell}{2}} = \alpha(0) \qquad \text{(A1.9)}$$

with ℓ the path length through the nucleus in the cylindrical approximation, and σ_T is the total cross section for πN scattering.

The angular distribution for the elastic nuclear scattering can be closely approximated by

$$\frac{d\sigma}{d\Omega} = |f_N(\theta)|^2 = e^{-\theta^2/2\theta_o^2} \; |f_N(0)|^2 \qquad \text{(A1.10)}$$

where $\theta_o \sim 1.4\, \lambda\!\!\!^{-}_{\pi}/R_N$. The real part of the amplitude is, therefore,

$$\mathrm{Re}(f_N(\theta)) = \alpha_N(\theta) \; \frac{(p/m_\pi)\sigma_T}{\lambda\!\!\!^{-}_{\pi} 4\pi} \; e^{-\theta^2/4\theta_o^2} \; .$$

The interference between the Coulomb and nuclear amplitudes results in the following change in cross section,

$$\Delta\sigma_{\pi\pm} = \pm \int 2\mathrm{Re}(f_N(\theta) * f_C(\theta))\, d\Omega \; . \qquad \text{(A1.11)}$$

To fold in the effects of the detector's efficiency changing as a function of angle, this integral is weighted by a factor $(1-e^{\theta^2/2\theta_A})$ where θ_A characterizes the efficiency of the detector for such scatterings. Using the results from (A1.7), letting the nuclear amplitude $\mathrm{Re}(f_N(\theta)) = \mathrm{Re}(f_N(0))g$ where g is the form factor of the nucleus we evaluate Eq. (A1.11) to get

$$\Delta\sigma = \frac{Z\, \alpha\, \lambda\!\!\!^{-}_{\pi}}{\beta\; p/m_\pi} \; \mathrm{Re}\{f_N(0)\} \; \frac{1}{2\theta_A^2} \int g^2 \, d\Omega \qquad \text{(A1.12)}$$

for $\theta_A << \theta$. This integral over the form factor can be related to the diffractive cross section of the nucleus σ_D and the α_N's to give an effective difference in π^+ and π^- absorption of

$$\Delta\sigma_{\mathrm{eff}} = \frac{Z\, \alpha\, 8\pi\, \lambda\!\!\!^{-2}_{\pi}}{(p/m_\pi)^2\, \theta_A^2} \; \frac{\sigma_D}{\sigma_T} \left(\frac{\alpha_N^{\pi+}}{(\alpha_N^{\pi+})^2 + 1} + \frac{\alpha_N^{\pi-}}{(\alpha_N^{\pi-})^2 + 1} \right) . \qquad \text{(A1.13)}$$

Inserting typical values into Eq. (A1.13); $\overline{Z} = 8$, $p/m_\pi \sim 10$, $\sigma_D/\sigma_T = 0.25$, $\theta_A \sim .1$ rad, $\alpha_N^{\pi+} = -.32$, $\alpha_N^{\pi-} = -0.09$ (for cross section values and $\alpha_N(0)$'s see Ref. 37) results in an effective difference in cross section of

$$\Delta\sigma_{eff} = (2.9 \pm .3) \text{ mbarns.}$$

This change in cross section produces a change in δ due to the differential loss of pions due to the mass of the detector, viz.,

$$\Delta\delta = (.33 \pm .03)*10^{-4} \quad .$$

C. K_L^o and Neutron Interactions

The interactions of K_L^o with the decay region material can produce a background that is highly charge asymmetric (viz., $\Lambda^o \rightarrow pe\nu$). The production cross sections for Λ^o's in this momentum region is roughly (38)

$$5*10^{-4} \ \Lambda^o/K_L^o \quad \text{per gram of material.}$$

This production rate coupled with a branching ratio of 10^{-3} for the $\Lambda^o \rightarrow pe\nu$ decay mode results in an insignificant contamination of δ,

$$\Delta\delta < \ 2.5*10^{-8}$$

from this process.

The effect of neutron interactions in the creation of a highly asymmetric background must also be considered. One possible scenario for such a background is $nN \rightarrow \pi^o pN$ where the π^o decays to a Dalitz pair. A typical cross section for this reaction is $\sim$ 20 μ barns. For this interaction to contaminate the good data, only the e^-p pair are seen by the spectrometer. This results in an estimate of the contamination per gram of material distributed uniformly throughout the decay region of $\sim 4*10^{-4}$ $nN \rightarrow e^+e^-\gamma pN$ reactions/K_{e3} trigger. Allowing for $\sim$ .10 g/cm^2 of the spectrometer upstream of the Čerenkov to contribute to this effect, a net change in the asymmetry of

$$\Delta\delta \ \underset{\sim}{} \ (2. \pm 1.)*10^{-5}$$

results.

As a further check on the level of contamination of the data due to beam interactions in the decay volume, several million events were recorded while having a 1 g/cm^2 piece of carbon in the decay region (Z = -120 inches). This carbon increased the material available for these interactions by a factor of ~ 20. However, due to the inbending/outbending difference the data downstream of the piece of material must be suitably corrected before a comparison can be made. After this correction is performed the asymmetry of the data downstream of this material is

$$\delta_{downstream} = (2.96 \pm 1.31)*10^{-3} .$$

Making an extrapolation for these two points, a change in the asymmetry of

$$\Delta\delta = (-.05 \pm .40)*10^{-3}$$

results. This change in asymmetry has a different sign, however, when considering the error in this result it is consistent with the magnitude of the effect predicted by the previous calculation.

D. Delta Ray Production

As an auxiliary test of problems which might arise from delta rays being produced in the Čerenkov mirrors and being reflected back into the Čerenkov light collecting buckets, a large sample of δ-rays were generated from a K_{e3} Monte Carlo distribution of intersections of pion trajectories with the Čerenkov mirrors. Electrons were generated at these impact points with energies consistent with a $1/E^2$ probability distribution and with a 17 MeV threshold for detection by the Čerenkov counter. The linear energy dependence factor in this production spectrum [39] has been neglected and the spectrum was truncated at energy E_{max} where

$$E_{max} = \frac{m_e c^2 \beta_\pi^2}{1 - \beta_\pi^2} .$$

The effect of this approximation was to allow a slightly larger number of higher energy δ-rays to appear in the spectrum which does not affect the results drastically. For each mirror impact position, 10 δ-rays each were generated on A and B polarity, and then each was stepped through the magnetic field integrating in 1/2-inch steps until they exit at the upstream side of the Čerenkov counter.

The information which was recorded for each event thus generated was; the polarity of the magnetic field for the δ-ray, the topology of the Monte Carlo event being used, the region in the counter where the δ-ray was reflected back into and whether the element struck during this reflection was consistent with the track location in the counter.

Approximately 200K such events were generated with the following results:

(1) 30% of the δ-rays end up in the wrong Čerenkov cell (i.e., would be considered Čerenkov inconsistencies).

(2) 69% of the δ-rays miss the light collector buckets all together (reflecting back out the front window and sides of the counter).

(3) 1% end up in the right Čerenkov cell and would be confused with a genuine K_{e3} trigger.

(4) the charge asymmetry for these events was $(-250. \pm 10.)*10^{-3}$.

This fairly low acceptance of these events coupled with the production cross section for delta rays in the mirror material results in a maximum contamination of the data by these events of the order of 10^{-4}. This type of fake signal results in a correction to the measured asymmetry of

$$\Delta\delta \leq (+2.5 \pm .1)*10^{-5} \quad .$$

In addition to this calculation for delta ray effects, auxiliary data were taken to explicitly study this model. To make this measurement the mirror material was increased a factor of 4 by placing extra sheets of Plexiglas behind the

As a further check on the level of contamination of the data due to beam interactions in the decay volume, several million events were recorded while having a 1 g/cm^2 piece of carbon in the decay region (Z = -120 inches). This carbon increased the material available for these interactions by a factor of ~ 20. However, due to the inbending/outbending difference the data downstream of the piece of material must be suitably corrected before a comparison can be made. After this correction is performed the asymmetry of the data downstream of this material is

$$\delta_{downstream} = (2.96 \pm 1.31)*10^{-3} .$$

Making an extrapolation for these two points, a change in the asymmetry of

$$\Delta\delta = (-.05 \pm .40)*10^{-3}$$

results. This change in asymmetry has a different sign, however, when considering the error in this result it is consistent with the magnitude of the effect predicted by the previous calculation.

D. Delta Ray Production

As an auxiliary test of problems which might arise from delta rays being produced in the Čerenkov mirrors and being reflected back into the Čerenkov light collecting buckets, a large sample of δ-rays were generated from a K_{e3} Monte Carlo distribution of intersections of pion trajectories with the Čerenkov mirrors. Electrons were generated at these impact points with energies consistent with a $1/E^2$ probability distribution and with a 17 MeV threshold for detection by the Čerenkov counter. The linear energy dependence factor in this production spectrum [39] has been neglected and the spectrum was truncated at energy E_{max} where

$$E_{max} = \frac{m_e c^2 \beta_\pi^2}{1 - \beta_\pi^2} .$$

The effect of this approximation was to allow a slightly larger number of higher energy δ-rays to appear in the spectrum which does not affect the results drastically. For each mirror impact position, 10 δ-rays each were generated on A and B polarity, and then each was stepped through the magnetic field integrating in 1/2-inch steps until they exit at the upstream side of the Čerenkov counter.

The information which was recorded for each event thus generated was; the polarity of the magnetic field for the δ-ray, the topology of the Monte Carlo event being used, the region in the counter where the δ-ray was reflected back into and whether the element struck during this reflection was consistent with the track location in the counter.

Approximately 200K such events were generated with the following results:

(1) 30% of the δ-rays end up in the wrong Čerenkov cell (i.e., would be considered Čerenkov inconsistencies).

(2) 69% of the δ-rays miss the light collector buckets all together (reflecting back out the front window and sides of the counter).

(3) 1% end up in the right Čerenkov cell and would be confused with a genuine K_{e3} trigger.

(4) the charge asymmetry for these events was $(-250. \pm 10.)*10^{-3}$.

This fairly low acceptance of these events coupled with the production cross section for delta rays in the mirror material results in a maximum contamination of the data by these events of the order of 10^{-4}. This type of fake signal results in a correction to the measured asymmetry of

$$\Delta\delta \leq (+2.5 \pm .1)*10^{-5} \quad .$$

In addition to this calculation for delta ray effects, auxiliary data were taken to explicitly study this model. To make this measurement the mirror material was increased a factor of 4 by placing extra sheets of Plexiglas behind the

Čerenkov counter. In order to evaluate the measured change in asymmetry due to these knock-on electron events, a subtraction must be made since in increasing the effective mass of the mirror material by 9, an overall increase in mass of the spectrometer by a factor of 3 also resulted. After doing this the measured effect was

$$\Delta\delta = (+.16 \pm .50)*10^{-3}$$

which is in reasonable agreement with the previous calculation.

In summary, the following mass correction is predicted for the asymmetry per .637 g/cm^2 of material in the spectrometer.

Positron Annihilation	$.15 \pm .001 * 10^{-3}$
Differential $\pi^+\pi^-$	
(1) I≠0	$.03 \pm .00015$
(2) I=0	$.09 \pm .0004$
(3) Coulomb Interference	$.033 \pm .003$
K_L^o, n Interactions	$.02 \pm .01$
Delta Ray Production	$.025 \pm .001$
total	$+.348 \pm .0104 * 10^{-3}$.

The errors quoted above are to illustrate only the error in the size of the effects that have been considered and do not reflect the uncertainty in these calculations which results from the approximations that were used.

APPENDIX 2

CENTER LINE INTERCEPT WINDOW CALCULATION

The process of track finding required that attention be given to the effects of the granularity of the detector in track reconstruction. Since there was only horizontal position information available in the spectrometer, one could treat this problem in the (X, Z) plane of the spectrometer. The analysis program when searching for possible tracks in the primary data constructed the intercept at the magnet center line (Z=0) from a pair of points in the chambers (X_i, Z_i), (X_j, Z_j) as follows,

$$X(Z=0) = X_i + \frac{X_i - X_j}{Z_i - Z_j} * Z_i \,. \qquad \text{(A2.1)}$$

Since the points (X_i) are taken to be at the center of the given spectrometer element there exist then a number of allowable intersections for a given pair of elements in the front or back of the spectrometer, and it is this spread in intersections that must be considered.

$$X_{Max} = (X_i - \delta X_i) + \frac{(X_i - \delta X_i) - (X_j + \delta X_j)}{Z_i - Z_j} * Z_i$$

$$X_{Min} = (X_i + \delta X_i) + \frac{(X_i + \delta X_i) - (X_j - \delta X_j)}{Z_i - Z_j} * Z_i$$

$$\Delta_{(ij)} \equiv |X_{Max} - X_{Min}| = -2\delta X_i + \frac{Z_i}{Z_i - Z_j} \left(-2\delta X_i - 2\delta X_j \right) \qquad \text{(A2.2)}$$

$$= 2\left(\delta X_i + \frac{Z_i}{Z_i - Z_j} \left(\delta X_i + \delta X_j\right)\right) \,.$$

Evaluating Eq. (A2.2) for the three possible front chamber configurations yields:

$$\Delta_X(1,2) = (.75" + \frac{87.12}{15.19} \quad (1.625)) = 10.06"$$

$$\Delta_X(2,3) = (.875" + \frac{71.93}{15.13} \quad (1.875)) = 9.73" \qquad \text{(A2.3)}$$

$$\Delta_X(1,3) = (.75" + \frac{87.12}{30.32} \quad (1.75)) = 5.84"$$

and for the back chambers one has similarly:

$$\Delta_X(4,5) = (1.185" + \frac{73.56}{32.45} \quad (1.185)) = 3.87".$$

Thus three different values for the allowable center line intersection matching for the three chamber configurations were used i.e.,

$\Delta_X(1,2) = \pm 6.97"$ points in chambers 1 and 2

$\Delta_X(2,3) = \pm 6.80"$ points in chambers 2 and 3

$\Delta_X(1,3) = \pm 4.85"$ points in chambers 1 and 3.

For tracks with points in all front chambers, the window for $\Delta_X(1,3)$ was used, since the error depends upon the lever arm being used in the track finding as is shown in Eq. (A2.2).

APPENDIX 3

CALCULATION OF EFFECTS OF APPARATUS BIASES ON MEASURED CHARGE ASYMMETRY

One of the first problems encountered when setting out to perform a measurement this sensitive is the effect of apparatus bias. Measuring the asymmetry without considering this source of difficulty could lead to large systematic corrections in the final result. The following conventions will be used

$N_{e^+} \equiv (1 + \delta)\ N/2$ the number of e^+K_{e3} decays for N K_{e3} decays

$N_{e^-} \equiv (1 - \delta)\ N/2$ the number of e^-K_{e3} decays for N K_{e3} decays

ε_{ijk} = detection efficiency for polarity i (A or B) for j a given side of the spectrometer (Left or Right) for k electron charge (+/-).

From this it is clear that if the apparatus had unity detection efficiency for all configurations (i.e., $\Sigma\varepsilon_{ijk} = 1$), then for a given number of N K_{e3} decays detected

$$\delta_{Observed} = \frac{N^+ - N^-}{N^+ + N^-} \left(\frac{(1 + \delta) - (1 - \delta)}{(1 + \delta) + (1 - \delta)} \right) \frac{\frac{N}{2}}{\frac{N}{2}} = \delta \ . \quad (A3.1)$$

It is of interest to see what results when measuring the charge asymmetry with a realistic detector under several different sets of operating conditions.

First, suppose one has made the measurement without reversing the magnetic field in the spectrometer. The following would result (assuming the polarity used was A) for

$$N^{\pm}\ (\text{detected}) = \Sigma_j \varepsilon_{Aj^{\pm}}\ (1 \pm \delta)\ \frac{N}{2}\ ;$$

then

$$\delta_{Observed} = \frac{N^+ - N^-}{N^+ + N^-} = \frac{\Sigma_j \{(\varepsilon_{Aj^+} - \varepsilon_{Aj^-}) + \delta(\varepsilon_{Aj^+} + \varepsilon_{Aj^-})\}}{\Sigma_j \{(\varepsilon_{Aj^+} + \varepsilon_{Aj^-}) + \delta(\varepsilon_{Aj^+} - \varepsilon_{Aj^-})\}} \quad (A3.2)$$

By defining the apparatus asymmetry for a given polarity ϕ^i as:

$$\phi^i \equiv \frac{\sum_k \varepsilon_{i1k} - \sum_k \varepsilon_{i2k}}{\sum_k \varepsilon_{i1k} + \sum_k \varepsilon_{i2k}}$$

the apparatus asymmetry for the two event topologies becomes

$$\phi^A_{\text{Inbending}} \equiv \frac{\varepsilon_{A1-} - \varepsilon_{A2+}}{\varepsilon_{A1-} + \varepsilon_{A2+}}$$

$$\phi^A_{\text{Outbending}} \equiv \frac{\varepsilon_{A1+} - \varepsilon_{A2-}}{\varepsilon_{A1+} + \varepsilon_{A2-}} \quad .$$

Substituting these quantities into Eq. (A3.2) results in

$$\delta_{\text{Observed}} = \frac{(R^A_{\text{Out}}\ \phi^A_{\text{Out}} - R^A_{\text{In}}\ \phi^A_{\text{In}}) + \delta}{1 + (R^A_{\text{Out}}\ \phi^A_{\text{Out}} + R^A_{\text{In}}\ \phi^A_{\text{In}})\ \delta}$$

$$\tilde{=} (R^A_{\text{Out}}\ \phi^A_{\text{Out}} - R^A_{\text{In}}\ \phi^A_{\text{In}}) + \delta \qquad \text{(A3.3)}$$

where $R^A_{\substack{\text{In}\\\text{Out}}}$ is the relative efficiency for detection of each of these topologies. It appears from this expression that if one could arrange his detector to have equal detection efficiency for these two topologies this effect should cancel. For the geometry of this experiment the ratio of inbending to outbending events was 3:1, and typical apparatus asymmetries of the order of 1% were realized. These effects could have resulted in a change in the measured asymmetry of $\Delta\delta \sim 7*10^{-3}$ had the magnetic field reversals not been made periodically during the experiment. The reversal of magnetic field in the spectrometer artificially creates the situation described above of equal acceptance for in- and outbending topologies. In reversing the magnetic field the events which were outbending consequently become inbending and vice versa. Thus by taking equal amounts of

data on A and B polarity the effects of the apparatus bias is removed, viz.,

$$\delta_{Observed} = (R^A_{Out}\ \Phi^A_{Out} - R^B_{Out}\ \Phi^B_{Out}) + (R^B_{In}\ \Phi^B_{In} - R^A_{In}\ \Phi^A_{In}) + \delta$$
$$= \delta\ .$$

The act of reversing the magnetic field may however result in small changes in detection efficiency of the Čerenkov counter or the back hodoscope which disturbs this assumed symmetry in the system in the above calculation. If however, one pursues this problem allowing for these changes in efficiency with polarity the following measurement of the charge asymmetry results. Defining the ratio of data taken on A and B polarities as $\rho = \alpha/\beta$ where $\alpha + \beta = 1$ and where slight changes in the efficiency as a function of polarity are parameterized as $\varepsilon^{BL^+}_R = \varepsilon^{AL^-}_R(1-\delta')$ and $\varepsilon^{BL^-}_R = \varepsilon^{AL^+}_R(1-\delta')$ the following measurement of the charge asymmetry results

$$\delta_{Observed} = \left(\left(\frac{1-\rho}{1+\rho}\right) + \frac{\delta'}{2}\right)(R^A_{Out}\ \Phi^A_{Out} - R^A_{In}\ \Phi^A_{In}) + \delta. \qquad (A3.4)$$

If there were a localized change in efficiency (e.g., in a particular Čerenkov element) this $\delta'/2$ would directly add to the measured asymmetry. Evaluating (A3.4) to calculate these effects on the final data sample one obtains the following:

(1) From the data $(1-\rho)/(1+\rho) = 1*10^{-3}$

(2) $\Phi^A_{In} \simeq 16*10^{-3}$, $\Phi^A_{Out} = -1.5*10^{-3}$

(3) An estimate of the change in efficiency of the Čerenkov counter results in a $\delta' \sim 2*10^{-5}$

(4) The ratio of inbending events to outbending events is 3:1.

Then for the xl mass data

$$\delta_{Observed} - \delta = (-.012 \pm .0004)*10^{-3}.$$

The above arguments are also valid for changes in the detection efficiency for

pions in the spectrometer. This becomes more evident by transforming the efficiencies defined at the outset to the detection of the pions instead of its accompanying electron, and by modifying ε_{ijk}. This change in ε_{ijk} corresponds to an interchange of the states of the indices j and k (i.e., j,(Right, Left); k, (π^-/π^+)). Having done this, the above relationships can be calculated for changes in the pion detection efficiency.

REFERENCES

1. J. Christenson, J. Cronin, V. Fitch, and R. Turlay, Phys. Rev. Letters 13, 138 (1964).

2. See, for example,
L. Wolfenstein, Theory and Phenomenology in Particle Physics, (Academic Press, New York, 1969) Vol. 1, pp. 218-261.

3. See, for example,
J.W. Cronin, Proc. of the Fourth Hawaii Topical Conference, 1971, to be published by University of Hawaii Press.

4. T. Wu and C.N. Yang, Phys. Rev. Letters 13, 380 (1964).

5. J.S. Bell and R.K.P. Zia, Nuclear Physics B17, 388 (1970).

6. J.C. Brodine, Nuclear Physics B30, 545 (1971).

7. S. Bennett, D. Nygren, H. Saal, J. Steinberger, and J. Sunderland, Phys. Rev. Letters 19, 993 (1967).

8. J. Marx, D. Nygren, J. Peoples, T. Kirk, and J. Steinberger, Phys. Letters 32B, 219 (1970).

9. V.A. Ashford, B.C. Brown, G.E. Masek, T. Maung, E.S. Miller, H. Ruderman, D.J. Shields, and W. Vernon, Phys. Letters 38B, 47 (1972).

10. D. Dorfan, J. Enstrom, D. Raymond, M. Schwartz, S. Wojcicki, D.H. Miller, and M. Paciotti, Phys. Rev. Letters 19, 987 (1967).

11. Robert L. McCarthy, "Measurement of the Charge Asymmetry in the Decay $K_L^o \to \pi\mu\nu$", Thesis, University of California, Berkeley, 1971 (unpublished).

12. M. Gell-Mann, Phys. Rev. 92, 833 (1953).

13. M. Gell-Mann and A. Pais, Phys. Rev. 97, 1387 (1955).

14. V.F. Weiskopf and E.P. Wigner, Z. Physik 63, 54 (1930); Z. Physik 65, 18 (1930)

15. K. Winter, Proc. of Amsterdam Conference, 1971.

16. T.D. Lee, R. Oehme, and C.N. Yang, Phys. Rev. 106, 340 (1957).

17. J.S. Bell and J. Steinberger, Proceedings of the International Conference on Elementary Particles, Oxford (1965).

18. G. Charpak and M. Gourdin, "The K^o- $\overline{K}^o$ System", CERN Report 67-18 (1967) (unpublished).

19. M.W. Strovink, "CP Violation and Regenerated K^0_{e3} Decay", Thesis, Princeton University, 1970 (unpublished).

20. G. Charpak, D. Rahm, and H. Steiner, Nucl. Instrum. and Methods 80, 13 (1970).

21. Aclar is a fluorocarbon film made by Allied Chemical Corporation (General Chemical Division), Morristown, N.J.

22. Purchased from Science Accessories Corp., 65 Station St., Southport, Conn.

23. Aluminizing of these mirrors was done by Denton Vacuum, Inc., Cherry Hill Industrial Center, Cherry Hill, N.J.

24. Purchased from New England Nuclear, Pilot Chemicals Division, 36 Pleasant St., Watertown, Mass.

25. J. Cronin, R. Cool, and A. Abashian, Phys. Rev. 107, 1121 (1957).

26. M. Crozens, Ph. Charanon, A. Courau, Th. Leray, J.L. Narjoux, and J. Tocqueville, Nuclear Physics 64, 567 (1965).

27. Edward S. Miller, "An Experimental Study of π^- - Nucleus Scattering from 0.6 to 1.6 BeV", Thesis, Princeton University, 1967 (unpublished).

28. J.S. Bell, Summer School of Theoretical Physics Les Houches (Grenoble) (Gordon and Breach Science Publishers, New York, 1965).

29. Review of older experiments by
M.K. Gaillard and L.M. Chounet, Phys. Letters 32B, 505 (1970).

30. C.-Y. Chien, E. Dally, P. Innocenti, E. Seppi, B. Cox, L. Ettlinger, L. Resvanis, R.A. Zdanis, C.D. Buchanan, D.J. Drickey, F.D. Rudnick, P.F. Shepard, D.H. Stork, and H.K. Ticho, Phys. Letters 35B, 261 (1971).

31. V. Bisi, P. Darriulat, M.I. Ferrero, C. Grosso-Pilcher, K. Kleinknecht, C. Rubbia, A. Staude, and K. Tittel, Phys. Letters 36B, 533 (1971).

32. P. Surko, M. Banner, J.W. Cronin, C.M. Hoffman, B.C. Knapp, and M.J. Shochet, Bull. of Amer. Phys. Soc. 17, 84 (1972).

33. V.L. Fitch, "CP Violation, Neutral Currents, and Weak Equivalence", Princeton University, PURC-4159-53, (unpublished).

34. J.M. Jauch and F. Rohrlich, The Theory of Photons and Electrons, (Addison-Wesley Publishing Company, Inc., Cambridge, Mass., 1955)Chap. 12, p.269.

35. H.A. Bethe, Annals of Physics 3, 190 (1958).

36. G. Höhler, G. Ebel, and J. Giesecke, Z. Physik 180, 430 (1964).

37. N.F. Mott and H.S.W. Massey, The Theory of Atomic Collisions, (Clarendon Press, Oxford, 1949), Ed. 2. Chap. III, p 48.

38. Particle Data Group, "A Compilation of $K^{+}N$ Reactions", UCRL-20000 (1969) (unpublished).

39. B. Rossi, High Energy Particles, (Prentice Hall Inc., New York, 1952) Chap.2, pp. 14-17.

LIST OF TABLES

TABLE I

Summary of Previous Charge Asymmetry Results

K_{e3} Asymmetry

H. Saal (Ref. 7) 1969

fully corrected $\delta = (2.24 \pm 0.36) * 10^{-3}$

lowest mass configuration = .733 g/cm^2
measured asymmetry = $(1.38 \pm 0.22) * 10^{-3}$
mass correction = $(0.86) * 10^{-3}$

J. Marx (Ref. 8) 1970

fully corrected $\delta = (3.46 \pm 0.33) * 10^{-3}$

lowest mass configuration = .875 g/cm^2
measured asymmetry = $(1.86 \pm 0.18) * 10^{-3}$
mass correction = $(1.55) * 10^{-3}$

V. Ashford (Ref. 9) 1971

fully corrected $\delta = (3.6 \pm 1.8) * 10^{-3}$

This Experiment 1971

fully corrected $\delta = (2.66 \pm .34) * 10^{-3}$

lowest mass configuration = .637 g/cm^2
measured asymmetry = $(1.99 \pm .29) * 10^{-3}$
mass correction = $(.54) * 10^{-3}$

$K_{\mu 3}$ Asymmetry

D. Dorfan (Ref. 10) 1967

fully corrected $\delta = (4.05 \pm 1.35) * 10^{-3}$

R. McCarthy (Ref. 11) 1971

fully corrected $\delta = (2.1 \pm 1.0) * 10^{-3}$

TABLE II

Neutral K Decay Rates

Decay Mode	K_S Rate†	K_L Rate†	$(\Gamma_{LF}\Gamma_{SF})^{1/2}/\delta M$*
$\pi^+\pi^-$	7960 ± 70	.0303 ± .001	2.88 ± .02
$\pi^o\pi^o$	3640 ± 60	.0182 ± .0037	1.55 ± .17
$2\pi(I=2)$			$\leq$.14
$\pi^+\pi^-\pi^o$	300	2.44 ± .06	.51 ± .005
$\pi^o\pi^o\pi^o$	?	4.14 ± .13	?
$\pi\mu\nu_\mu$	Same as K_L	5.20 ± .12	$\leq$.96 ± .02
$\pi e\nu_e$		7.52 ± .14	$\leq$1.39 ± .03
		total	$\leq$7.43 ± .20

Thereby implying:

$$|\langle L|S\rangle| \leq (7.43 \pm .20) * 10^{-3}$$

† Decay rates are given in units of $10^6 sec^{-1}$

* This ratio of rates is evaluated and the result is given in units of 10^{-3}

TABLE III

Collimator Data†

	#1	#2	#3
Length	46.5	42.0	48.0
Distance from target at entrance	145.5	375.0	732.0
Entrance horizontal aperture	0.942	2.039	3.745
Exit horizontal aperture	1.187	2.144	3.862
Entrance vertical aperture	1.798	4.639	9.045
Exit vertical aperture	2.375	5.152	9.642

† All dimensions are in inches.

TABLE IV

Proportional Chamber Data†

	1	2	3	4	5
Active Height (centered on beam)	16	16	16	25	30.5
Active width (per side)	12	14	16	36	36
Beam hole	0	1	2	5.725	10.5
Number of channels (per side)	16	16	16	32	32
Channel width	.75	.875	1.0	1.125	1.125
Longitudinal position along Z axis (as measured from magnet center)	-87.12	-71.93	-56.80	41.11	73.56
Wire size					
Signal plane	.0008[a]	.0025[b]	.0008	.0025	.0025
High voltage plane	.0025	.0025	.0025	.0025	.005[c]
Wire separation	0.125				
Plane spacing	0.25				

† All dimensions are in inches
a .0008" gold plated tungsten wire
b .0025" silver plated copper berylium wire
c .005" aluminum wire

TABLE V

Čerenkov Counter Data†

	Material	Height	Width or Dia.	Thickness
Entrance window	Mylar	18	34	0.0025
Exit window	Mylar	18	57.7	0.0025
Rectangular focussing mirrors	plexiglass	16	13	0.031
Flat trapezoidal mirrors (light collecting buckets)	glass	25	11.25 4.25	0.125
Outer magnetic shield	Armco iron	30	11.5	0.125
Inner magnetic shield	"Netic"	24	9.5	0.031
Radiator length		30		
Phototubes		(4) RCA 4522		

† All dimensions are in inches

TABLE VI

Scintillation Counter Data†

	E	F	M_{1-4}	B_{1-8}	NM^{*}_{X-Z}
Height	15	16	1.5	30	1
Width	24	6.5	36	9	1
Thickness	.062	.125	.375	.125	.125
Longitudinal position (as measured from magnet center)	-204.81	-25.0	15.0	79.45	-300
Beam hole		55.0		11.0	
Center above beam height			±9.25		
Phototube(RCA)	8575(2)	7746	7746	7746	7746

† All dimensions are in inches

* This array of counters was located in the beam and was used as a neutron monitor during the experiment.

TABLE VII

MASS DISTRIBUTION†

(x1 Mass Configuration)

	He	A-CO_2	Air	CO_2	Mylar	Aclar	Lucite	Pilot-B
Chemical Composition		2A-3CO_2	$\sim N_4O$		$C_5A_4O_2$	C_2ClF_3	$C_5O_2H_8$	C_9H_{10}
Decay Volume He Bag	.0118		.0025		.004			
Chamber 1		.0058				.0215		
He Bag	.0061		.001		.007			
Chamber 2		.0058				.0215		
He Bag	.0061		.001		.007			
Chamber 3		.0058				.0215		
Air Gap			.0025					
Čerenkov Counter				.150	.018		.117	
He Bag	.030				.007			
Chamber 4		.0047				.0215		
He Bag	.014				.007			
Chamber 5		.0047				.0215		
Air Gap			.0165					
Back Hodoscope								.0825 +.011 a
Totals	.068	.027	.024	.150	.050	.108	.117	.093

Grand Total .637 g/cm^2

† All quantities expressed in units of g/cm^2.
a Counter wrappings.

TABLE VIII

BREAKDOWN OF DATA ANALYSIS

Events on Primary Tape Processed	$96.0*10^6$
Events Reconstructed and Consistent with K_{e3} Signature	$85.3*10^6$
Categories of Events (Reconstructed)	
A. Beam Anti Tagged	3.7%
B. Magnet Anti Tagged	11.5%
C. Čerenkov Inconsistency	0.9%
D. Hodoscope Inconsistency	0.3%
E. Similar Bending	1.2%
F. Greater Than One Track on a Side	22.0%
Data Surviving Cuts A-E	$71.0*10^6$
Further Data Lost by Initial Cuts	
A. One or Both Particle Has Momentum > 2320 MeV/c	19.0%
B. Electron Momentum p_e < 200 MeV/c; Pion Momentum p_π < 500 MeV/c	9.7%
C. Center-line Crossing of One or Both Tracks < ±6 inches	6.9%
D. Horizontal Vertex (X) > ±3 inches	0.6%
E. Longitudinal Vertex (Z) < -185 inches	6.2%
Total Data Surviving Cuts	$41.0*10^6$

TABLE IX

SUMMARY OF DATA PASSING FINAL CUTS

Spectrometer Mass	Electron Charge	N_A^L	N_A^R	N_B^L	N_B^R	Apparatus Asymmetry (10^{-3})	Charge Asymmetry (10^{-3})
X 1 MASS ($0.637\ g/cm^2$)	N^+	781 245[a]	2 239 846[b]	2 308 408[a]	783 344[b]	IN = 16.12 ± .23	IN = 2.02 ± .33
	N^-	2 303 833[b]	780 638[a]	777 958[b]	2 226 079[a]	OUT = -1.53 ± .56	OUT = 1.92 ± .56
						TOTAL = 11.6 ± .28	TOTAL = 1.99 ± .28
X 4 MASS ($2.490\ g/cm^2$)	N^+	203 639	589 652	596 488	203 973	IN = 12.42 ± .64	IN = 0.34 ± .64
	N^-	603 974	207 404	199 866	581 341	OUT = -9.66 ±1.10	OUT = 0.41 ±1.10
						TOTAL = 6.77 ± .56	TOTAL = 0.36 ± .56
X 8 MASS ($4.780\ g/cm^2$)	N^+	188 659	543 444	556 636	186 927	IN = 17.96 ± .67	IN =-1.08 ± .67
	N^-	564 420	190 373	187 415	538 051	OUT = -1.63 ±1.15	OUT =-2.96 ±1.15
						TOTAL = 12.96 ± .58	TOTAL =-1.55 ± .58

Summary of Extrapolated Data

Inbending = $(2.55 \pm .39) * 10^{-3}$
Outbending = $(2.67 \pm .67) * 10^{-3}$
Total = $(2.53 \pm .34) * 10^{-3}$

[a] Inbending Data
[b] Outbending Data

LIST OF FIGURES

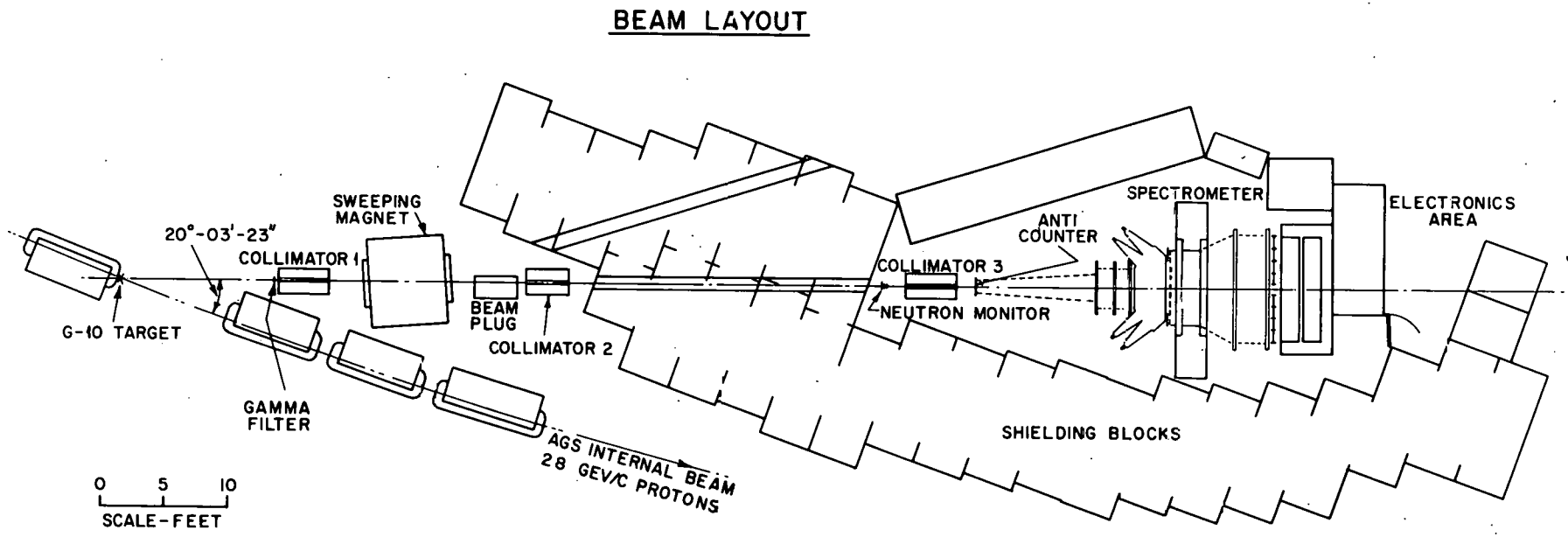
BEAM LAYOUT
SWEEPING MAGNET
20°-03'-23"
COLLIMATOR 1
BEAM PLUG
COLLIMATOR 2
G-10 TARGET
GAMMA FILTER
AGS INTERNAL BEAM
28 GEV/C PROTONS
0 5 10
SCALE-FEET
ANTI COUNTER
COLLIMATOR 3
NEUTRON MONITOR
SPECTROMETER
ELECTRONICS AREA
SHIELDING BLOCKS

Figure 1.

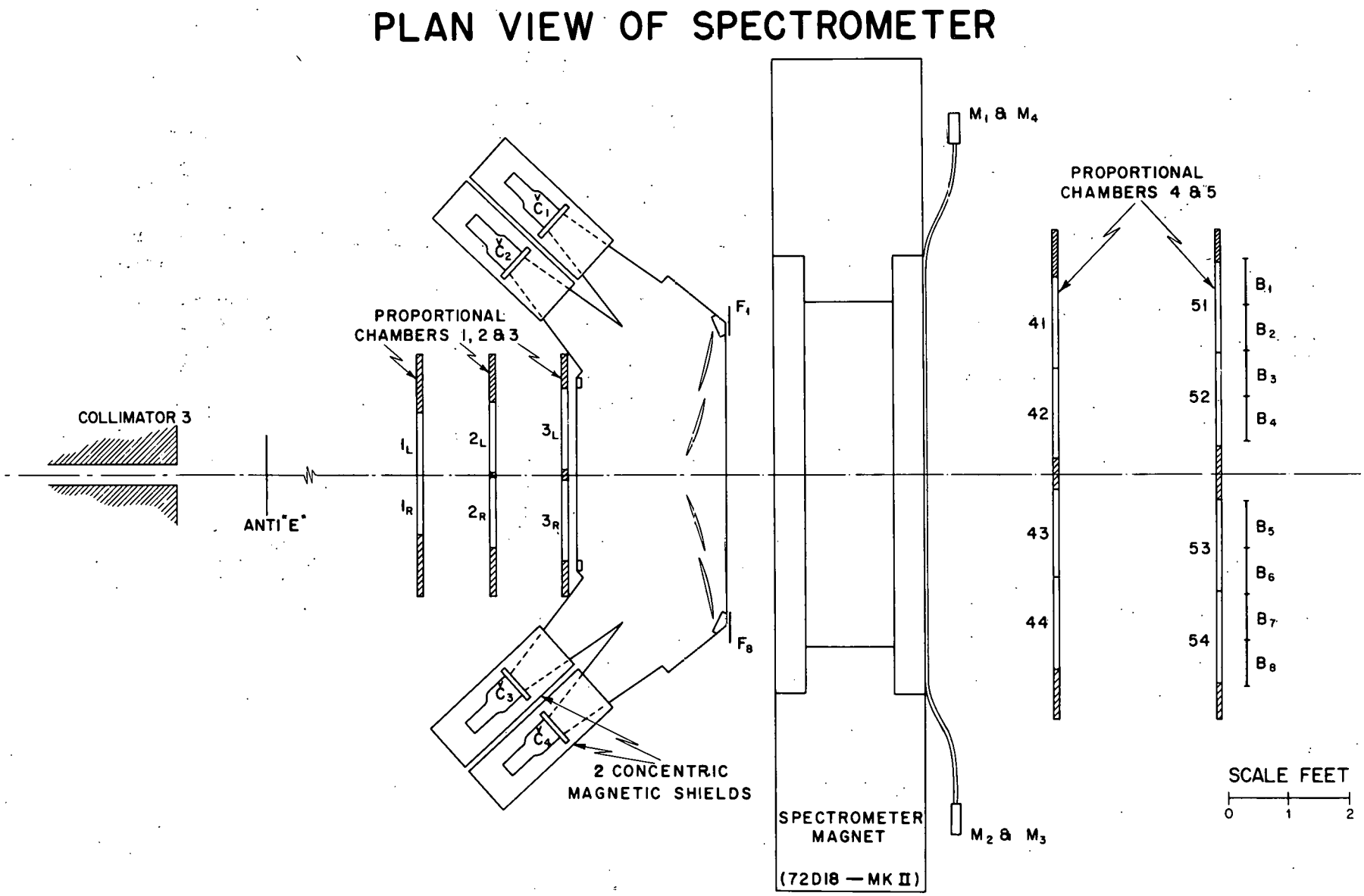
PLAN VIEW OF SPECTROMETER
M1 & M4
PROPORTIONAL CHAMBERS 4 & 5
C1
C2
F1
PROPORTIONAL CHAMBERS 1, 2 & 3
41
51
B1
B2
B3
B4
COLLIMATOR 3
1L
2L
3L
42
52
ANTI "E"
1R
2R
3R
43
53
B5
B6
B7
B8
44
54
F8
C3
C4
2 CONCENTRIC MAGNETIC SHIELDS
SPECTROMETER MAGNET
(72D18 — MK II)
M2 & M3
SCALE FEET
0
1
2

Figure 2.

AMPLIFIER AND DISCRIMINATOR CIRCUIT FOR PROPORTIONAL CHAMBER

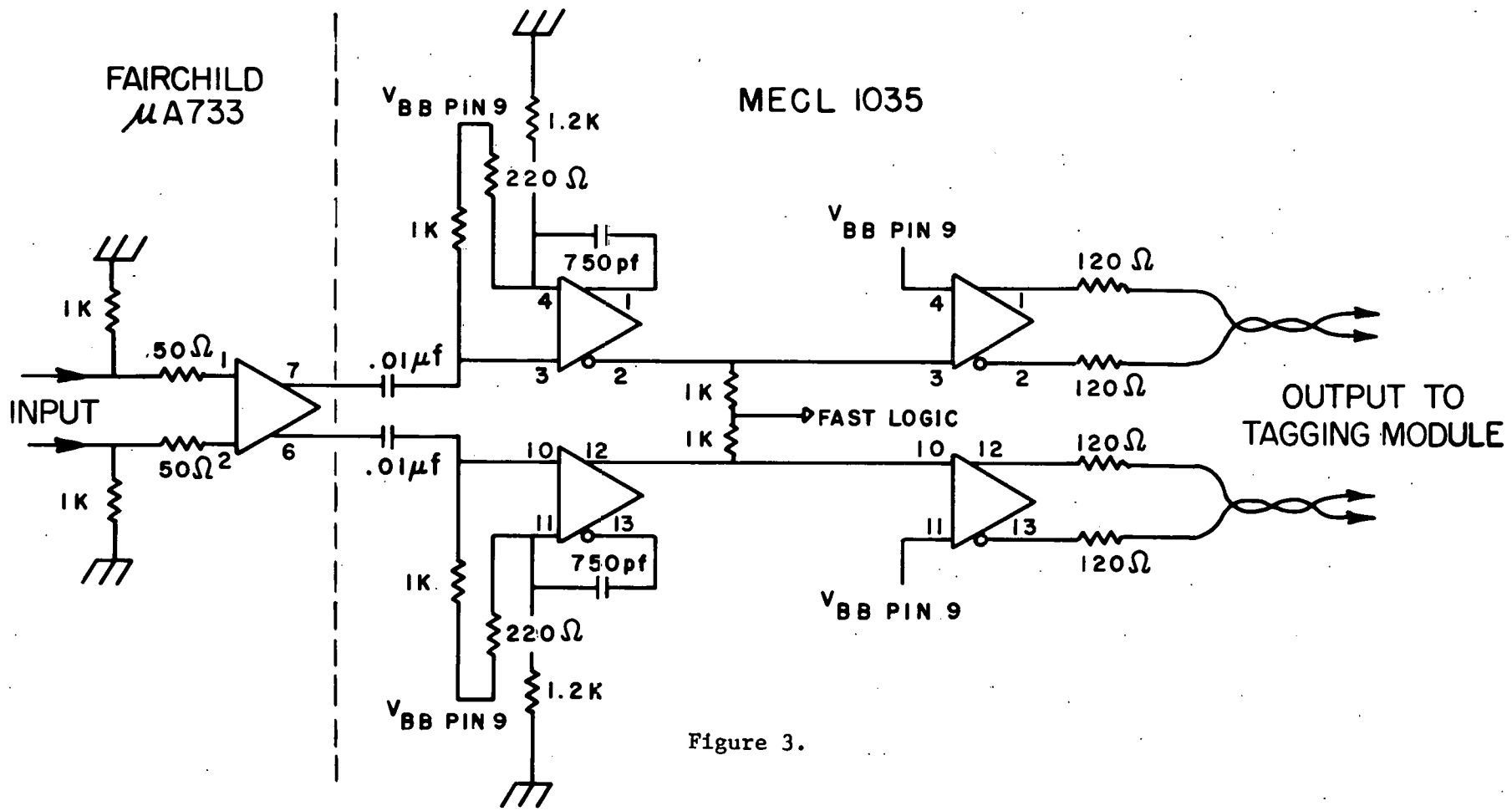

Figure 3.

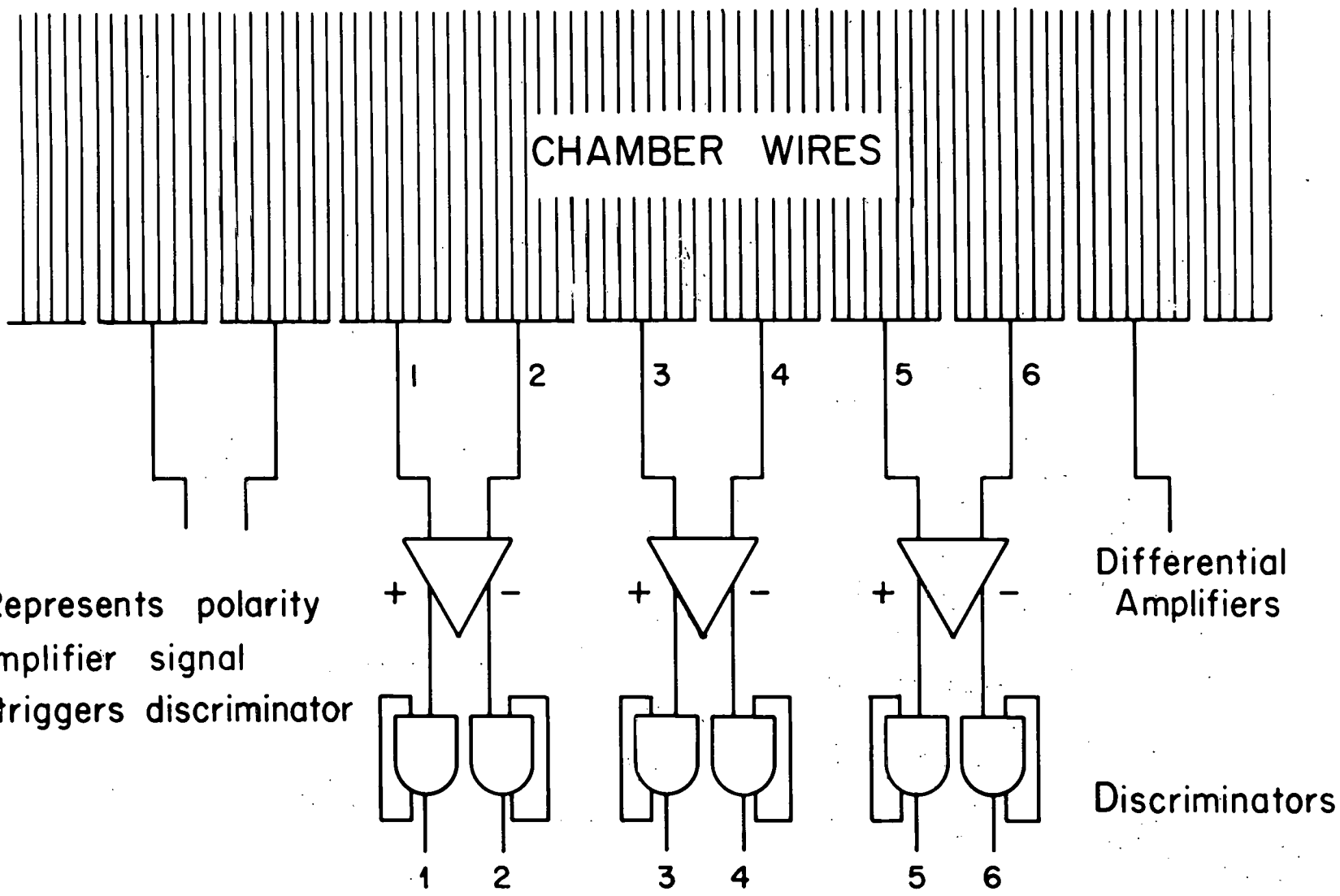

TYPICAL ELECTRONICS CONFIGURATION
FOR PROPORTIONAL CHAMBERS

Figure 4.

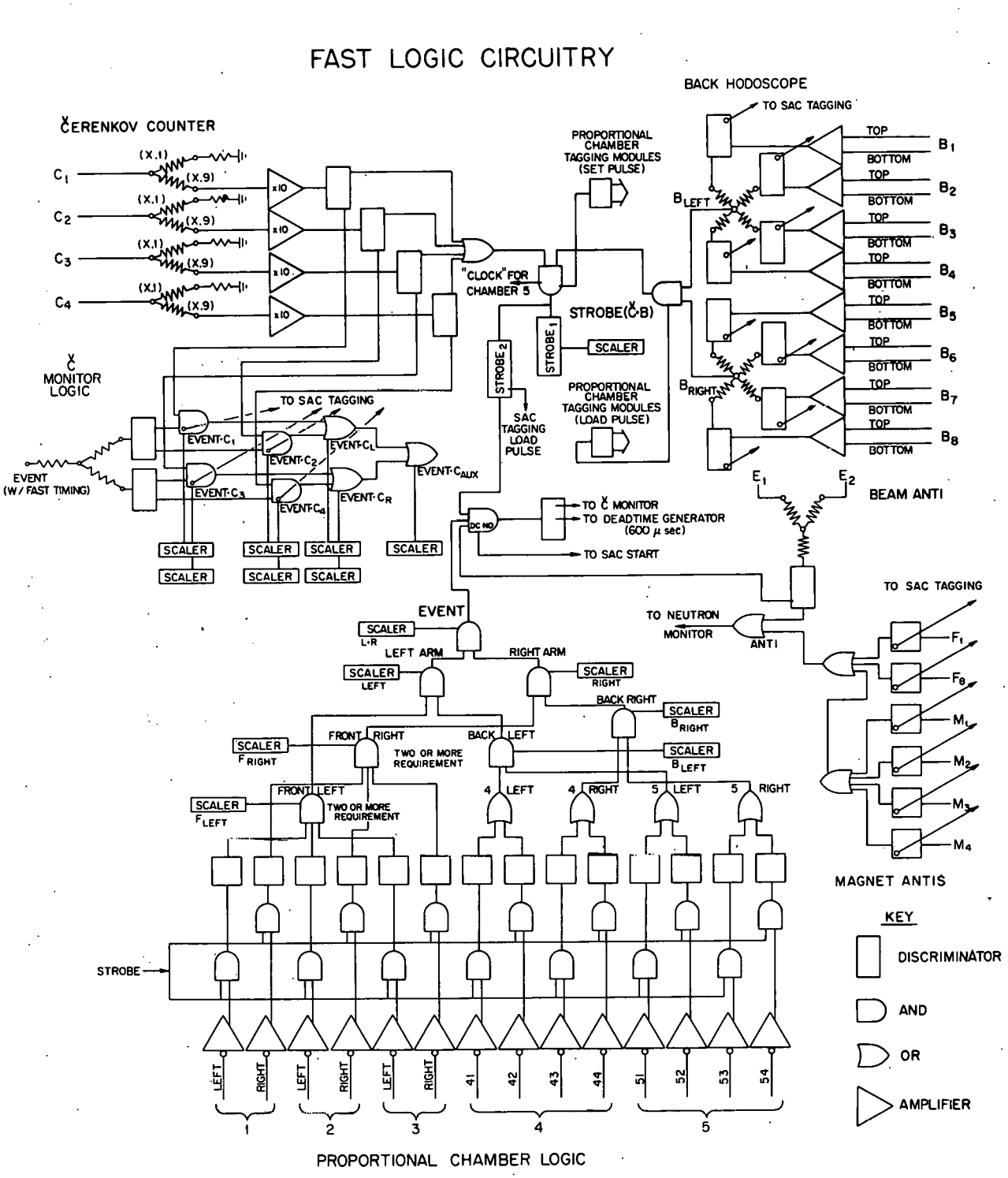
FAST LOGIC CIRCUITRY
BACK HODOSCOPE
TO SAC TAGGING
ČERENKOV COUNTER
PROPORTIONAL CHAMBER TAGGING MODULES (SET PULSE)
"CLOCK" FOR CHAMBER 5
STROBE(Č·B)
SCALER
Č MONITOR LOGIC
PROPORTIONAL CHAMBER TAGGING MODULES (LOAD PULSE)
SAC TAGGING LOAD PULSE
EVENT (W/ FAST TIMING)
TO Č MONITOR
TO DEADTIME GENERATOR (600 μ sec)
TO SAC START
BEAM ANTI
TO NEUTRON MONITOR
ANTI
EVENT
L·R
LEFT ARM
RIGHT ARM
LEFT
RIGHT
BACK RIGHT
FRONT RIGHT
BACK LEFT
TWO OR MORE REQUIREMENT
FRONT LEFT
4 LEFT
4 RIGHT
5 LEFT
5 RIGHT
STROBE
MAGNET ANTIS
KEY
DISCRIMINATOR
AND
OR
AMPLIFIER
PROPORTIONAL CHAMBER LOGIC

Figure 5.

SCHEMATIC OF DATA READOUT SYSTEM

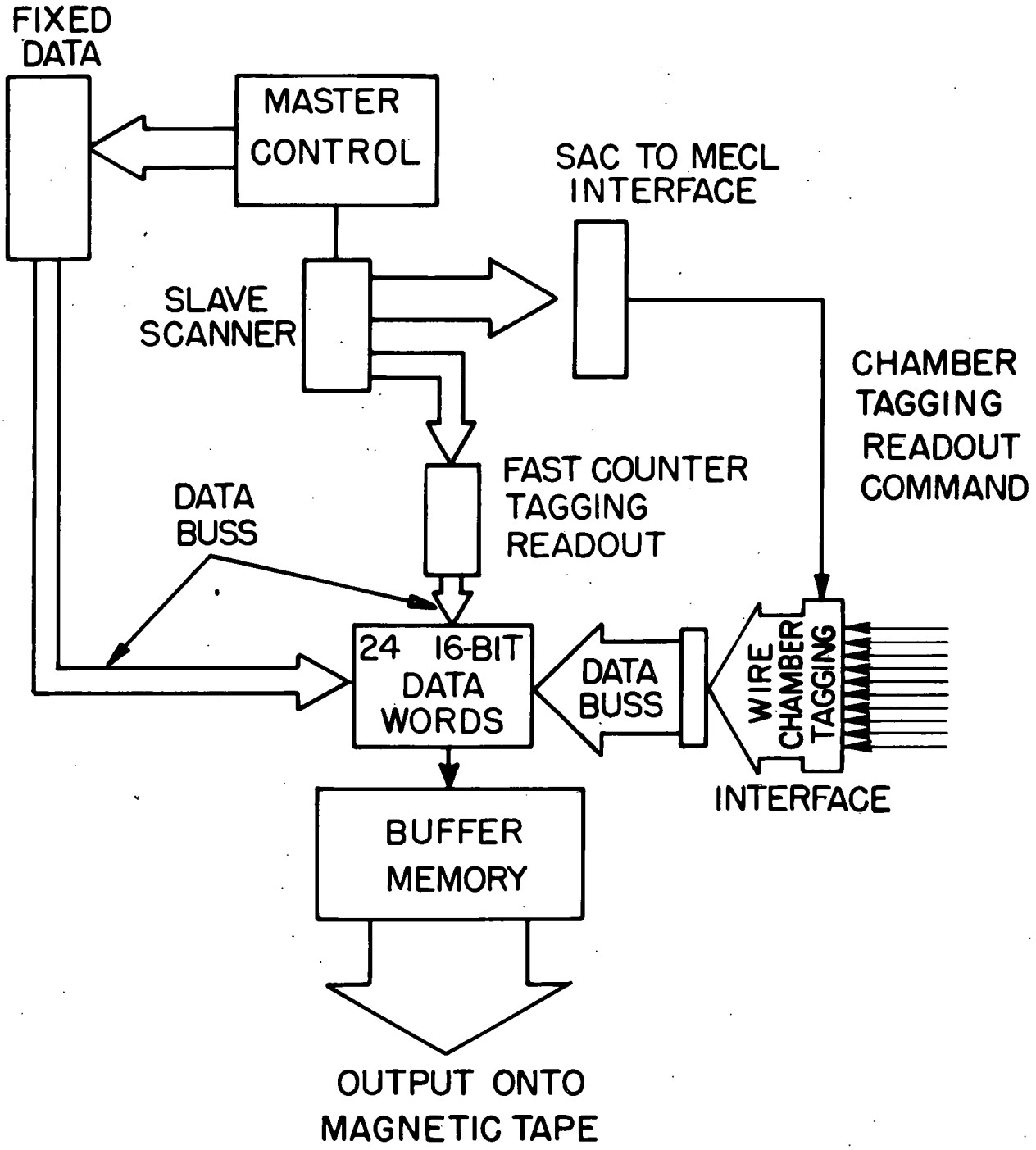

Figure 6.

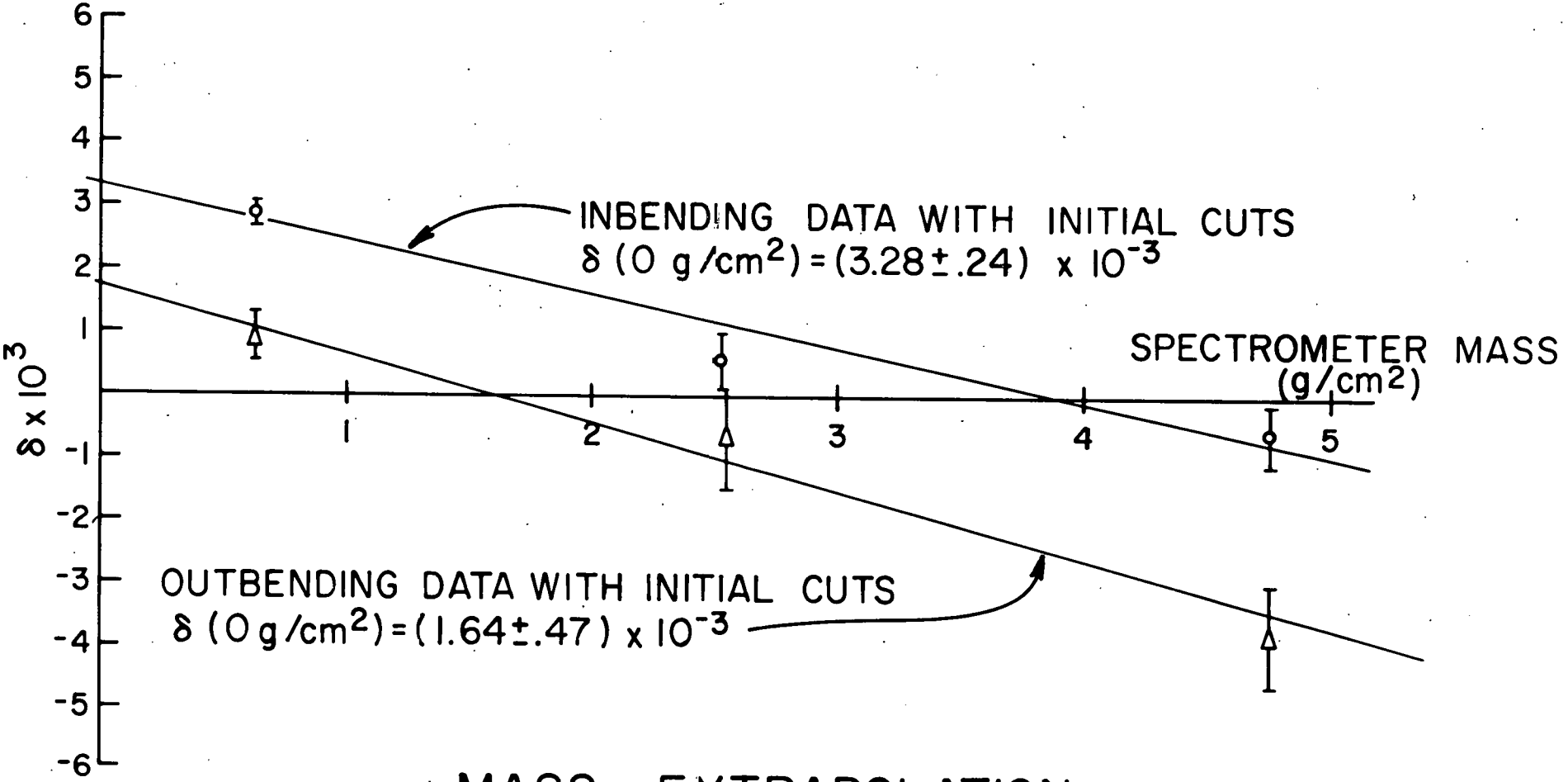

MASS EXTRAPOLATION
FOR DATA WITH CUTS

Figure 7.

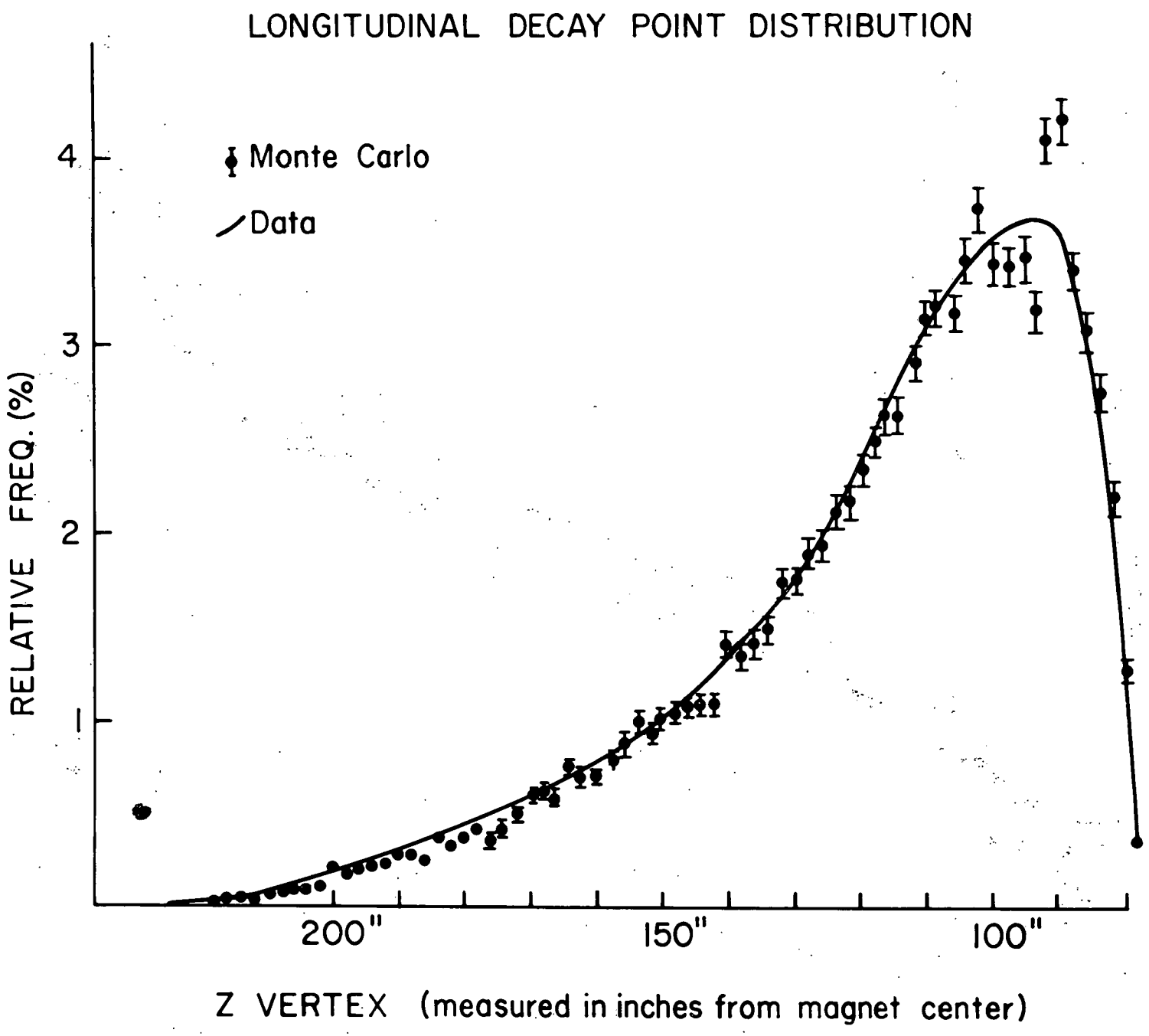
LONGITUDINAL DECAY POINT DISTRIBUTION
Monte Carlo
Data
RELATIVE FREQ. (%)
4
3
2
1
200"
150"
100"
Z VERTEX (measured in inches from magnet center)

Figure 8.

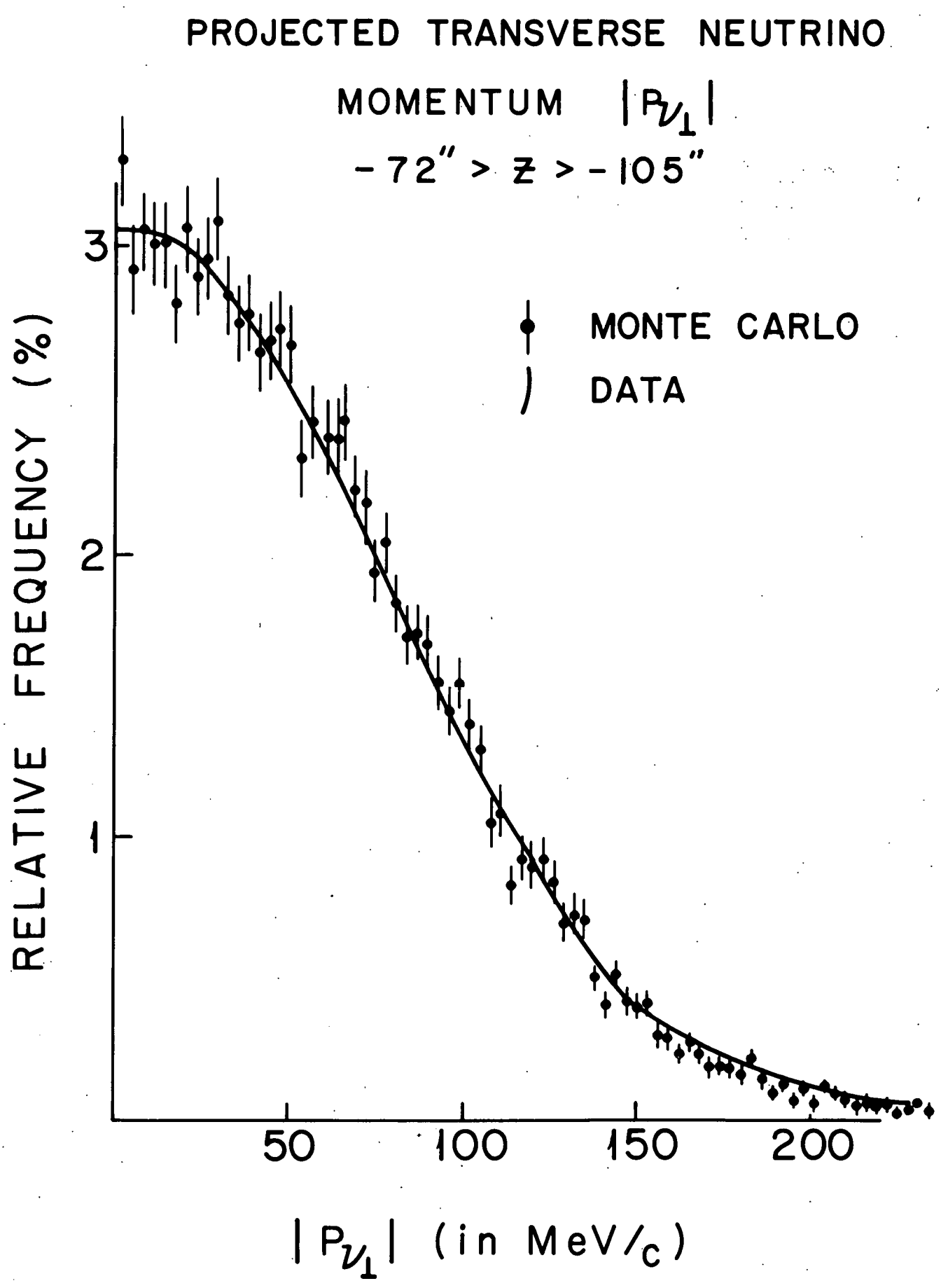
PROJECTED TRANSVERSE NEUTRINO
MOMENTUM $|P_{\nu_\perp}|$
$-72'' > z > -105''$
MONTE CARLO
DATA
RELATIVE FREQUENCY (%)
3
2
1
50
100
150
200
$|P_{\nu_\perp}|$ (in MeV/c)

Figure 9a.

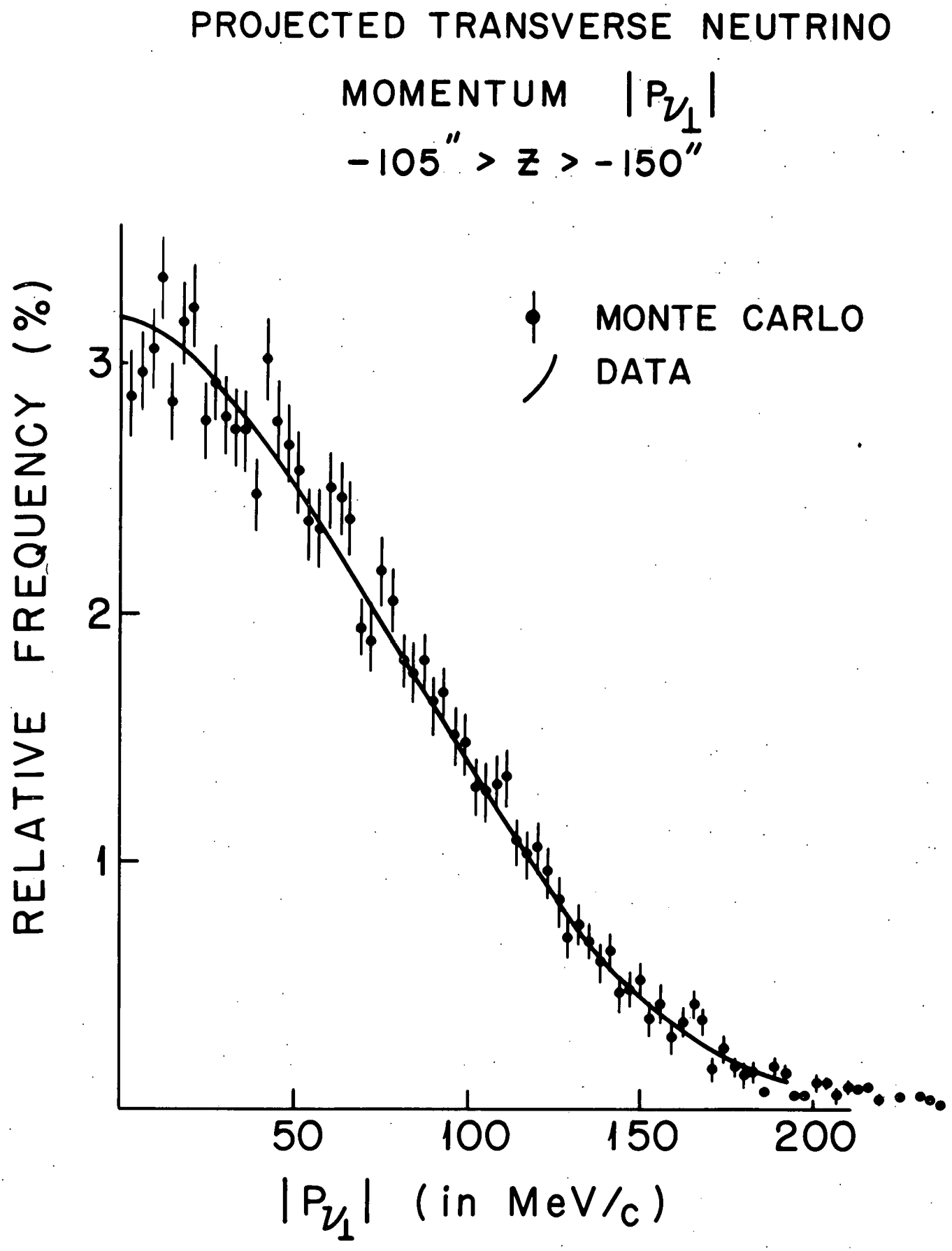
PROJECTED TRANSVERSE NEUTRINO
MOMENTUM $|P_{\nu_\perp}|$
$-105'' > z > -150''$
MONTE CARLO
DATA
RELATIVE FREQUENCY (%)
3
2
1
50
100
150
200
$|P_{\nu_\perp}|$ (in MeV/c)

Figure 9b.

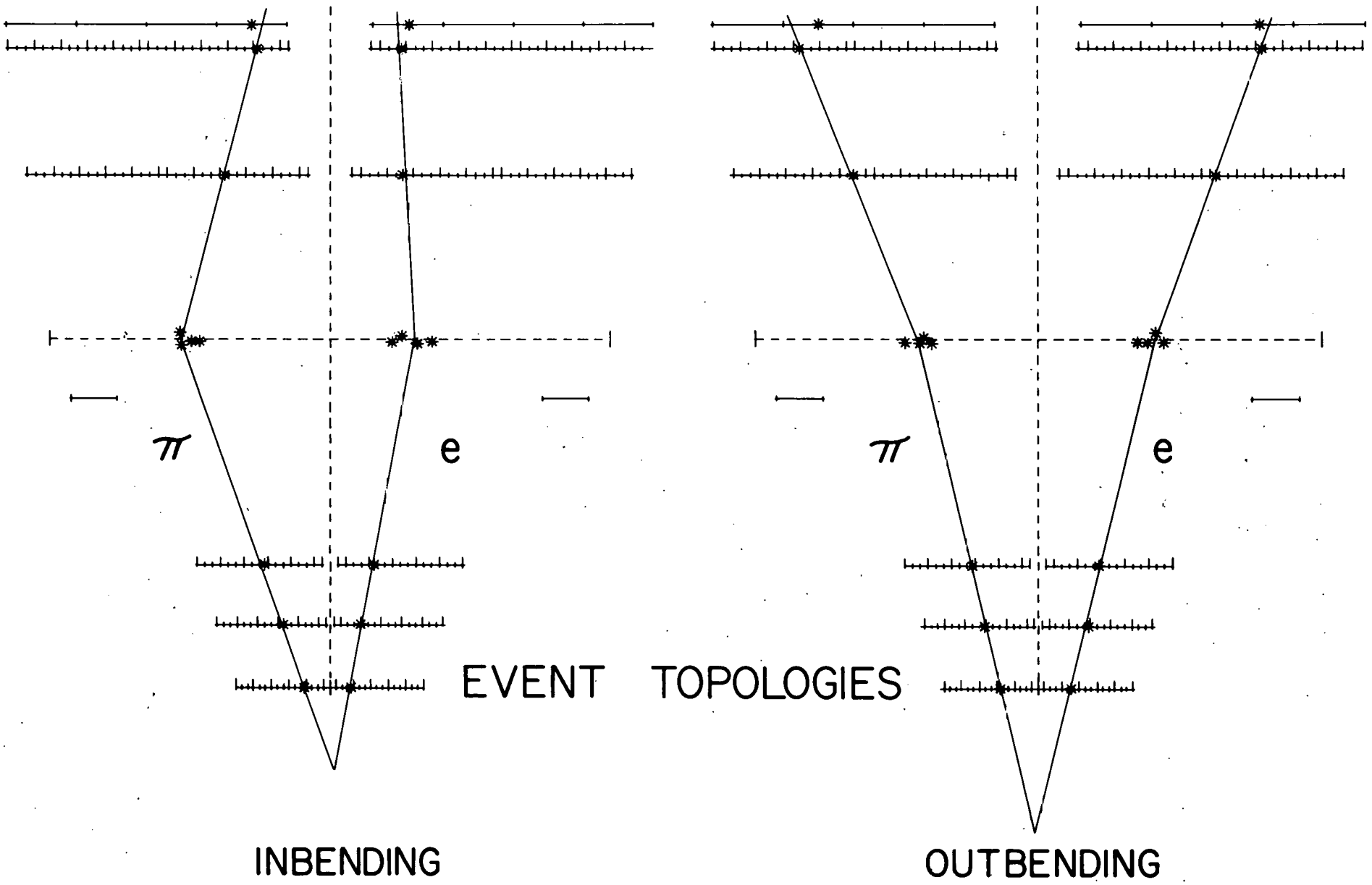

Figure 10.

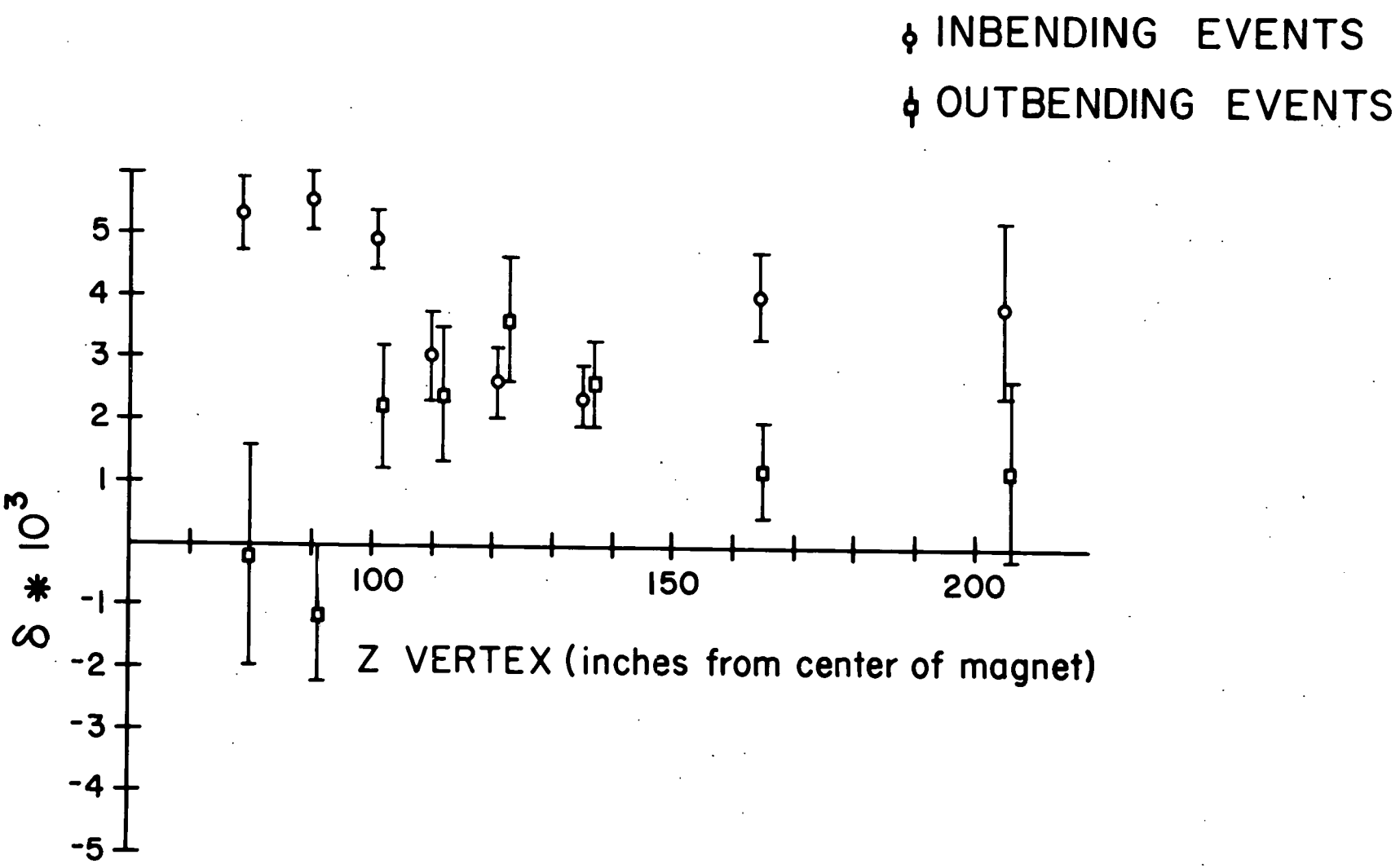

EXTRAPOLATED ASYMMETRY
FOR IN/OUTBENDING EVENTS AS
A FUNCTION OF Z VERTEX

Figure 11.

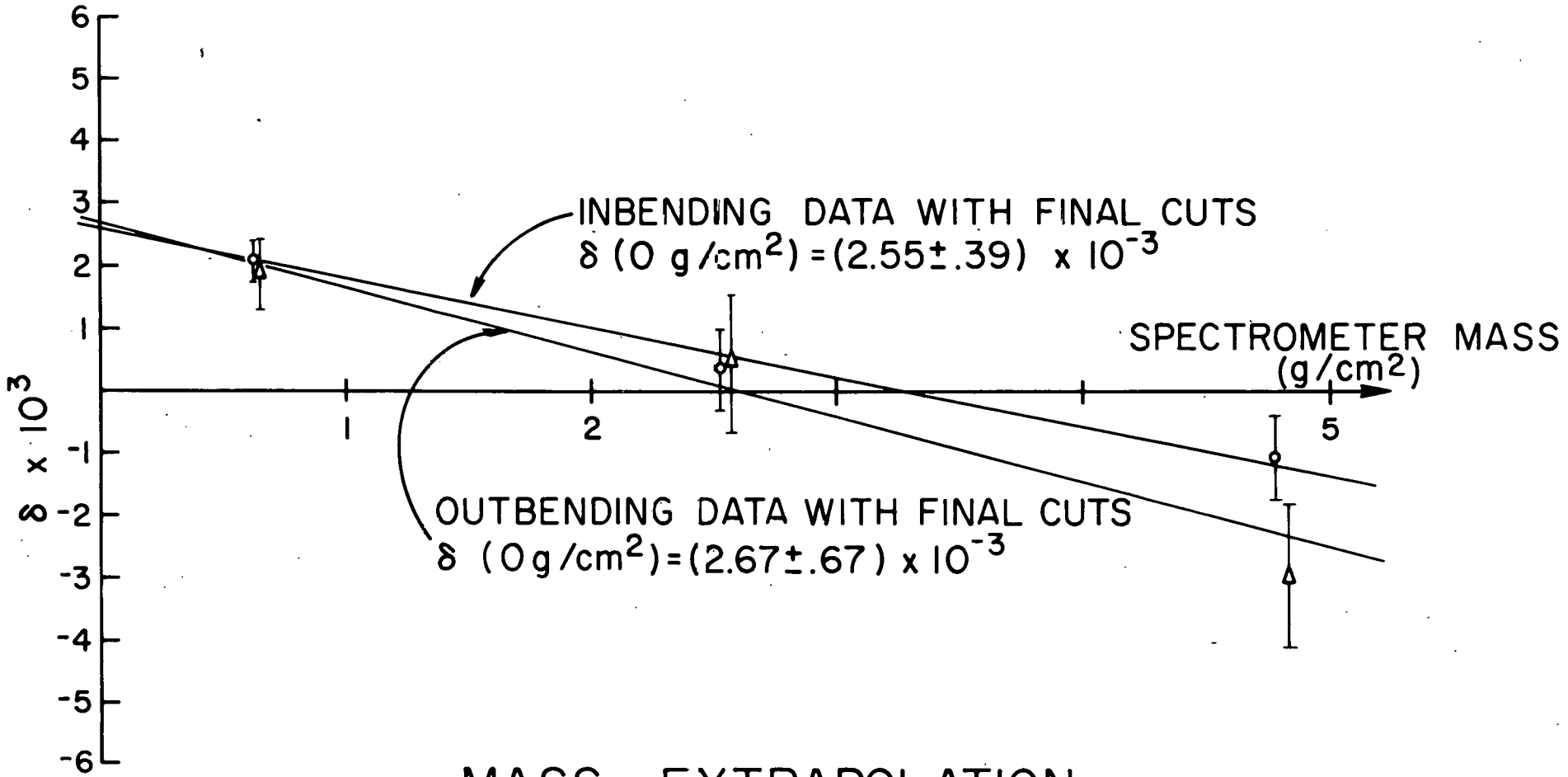

MASS EXTRAPOLATION
FOR DATA WITH CUTS

Figure 12.

Z VERTEX BEHAVIOR OF EXTRAPOLATED ASYMMETRY

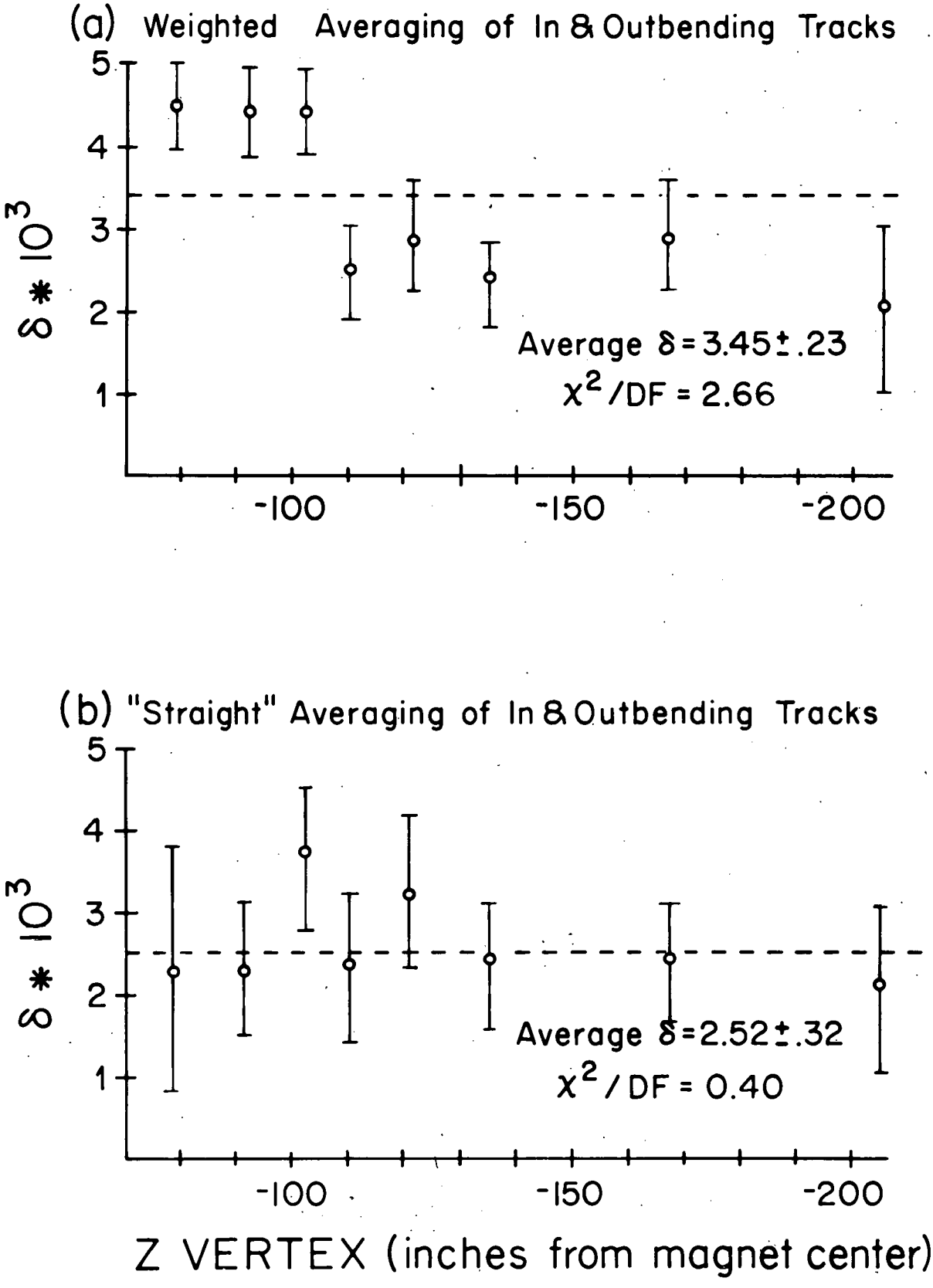

Figure 13.

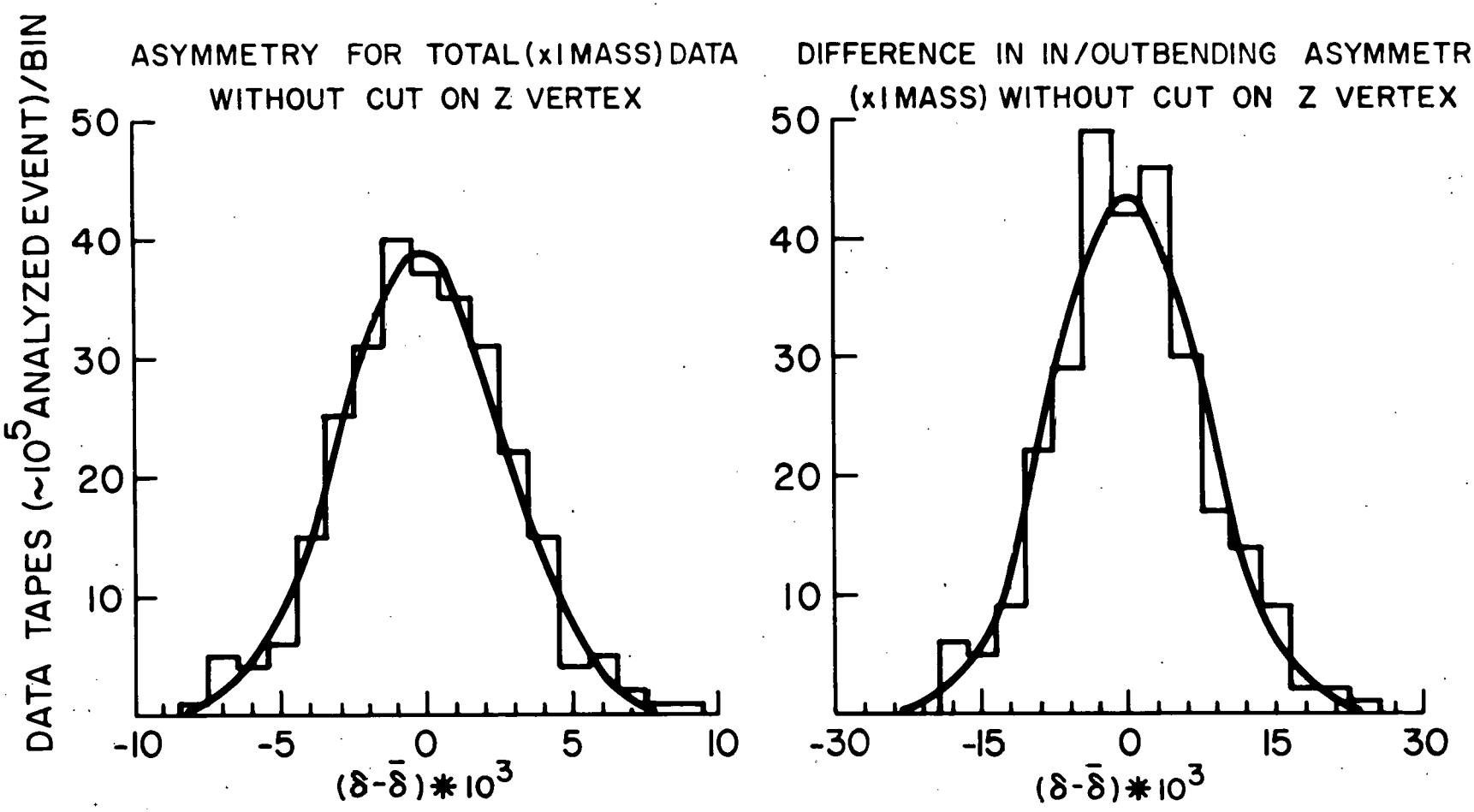

FITTED VALUES FOR GAUSSIAN DISTRIBUTION

(a) $\bar{\delta} = (2.36 \pm .17) * 10^{-3}$

$\sigma = (2.73 \pm .1) * 10^{-3}$

(b) $\bar{\delta} = (1.91 \pm .45) * 10^{-3}$

$\sigma = (7.45 \pm .27) * 10^{-3}$

DISTRIBUTION OF CHARGE ASYMMETRIES MEASURED FOR EACH PAIR OF POLARITY REVERSALS

Figure 14.